https://doi.org/10.1016/j.buildenv.2020.107429

Numerical evaluation of pedestrian-level wind comfort around "lift-up" buildings with various unconventional configurations

Lan Chen, Cheuk Ming Mak*

Department of Building Services Engineering, The Hong Kong Polytechnic University, Hung Hom, Hong Kong, China

***Corresponding author: Cheuk Ming Mak**

Email address: cheuk-ming.mak@polyu.edu.hk.

Abstract

Lift-up design can increase building permeability without sacrificing land use, and its effectiveness for pedestrian-level wind (PLW) comfort improvement has been confirmed. However, the subjects of previous studies are primarily rectangular- or square-plan building models. Modern buildings are not uniform but have various configurations, which exhibit different aerodynamic features. The PLW comfort around an isolated lift-up building with various unconventional configurations has not yet been systematically investigated. This study thereby aims to fill the research gap. A series of computational fluid dynamics simulations were performed to evaluate the PLW comforts around lift-up building models with 22 unconventional configurations. The tested configurations include polygonal, slab-like, cruciform, trident, and assembled models, derived from existing buildings in Hong Kong. The results indicate that the PLW comfort around an isolated building is sensitive to the incident wind direction, building configuration, and precinct size. Lift-up design can dramatically improve PLW comfort in the near field of a building. However, the improvement efficiency weakens with the wider size of the research region. The impact of lift-up design on the full-field wind comfort around a building may become negligible or negative. Several configuration parameters were identified, including the number of sides, projected width, building depth, included angle, converging and diverging flows, surface curvature, and surface discontinuity. Their impacts on the PLW comfort and lift-up design's comprehensive effectiveness were also justified. These findings can considerably enrich the knowledge of lift-up design's performance for wind comfort improvement, and contribute to creating a sustainable and livable microenvironment.

Keywords: Pedestrian-level wind comfort, Lift-up design, Building configuration, CFD simulation.

1. Introduction

The pedestrian-level wind (PLW) environment has attracted enduring attention since the late 20th century. On one hand, the mechanical effects of wind force on people (i.e. wind comfort) determine human activity forms[1]. For instance, sitting, strolling, and walking fast require different wind comfort levels[1]. On the other hand, wind condition is a key environmental factor affecting the urban living quality. Owing to rapid urbanization, modern cities are characterized by dense populations, tall buildings, and compact space. Therefore, the weak wind condition at the pedestrian level has become a pressing wind-related issue for many high-density cities over the past two decades. For instance, the annual mean wind speed over urban areas in Hong Kong underwent a steady decline of 0.2 m/s per decade between 1996 and 2015[2]. Low wind speed contributes to many environmental problems[3-13], including poor ventilation, heat and pollutant accumulation, worsening air quality, enhanced urban heat island effect, and outdoor thermal discomfort. More severely, poor air circulation provides beneficial conditions for airborne transmission of infectious diseases, such as the Coronavirus disease 2019 pandemic[14-18], Middle East respiratory syndrome[19], severe acute respiratory syndrome[20], and influenza[21]. Therefore, the imperative of solving various environmental issues and creating a comfortable microenvironment is to improve the low wind velocity at the pedestrian level.

Tropical and subtropical densely populated cities, such as Hong Kong and Singapore, are facing increased pressure on improving the PLW environment for concurrent heat stress and thermal comfort issues. The annual mean temperature in Hong Kong showed a rising trend of 0.13°C per decade during 1885–2019[22]. Furthermore, the increasing rate sped up, reaching 0.21°C per decade in the past 30 years[22]. To improve urban sustainability and livability, the Hong Kong SAR government issued the air ventilation assessment scheme of “the more wind the better”[23]. Later, Du et.al proposed a new wind criterion that suitable for the weak wind condition, which was based on the threshold mean wind velocity and the maximum exceedance probability[1].

Compact and bulky buildings are the primary causes of wind blockage in urban areas[24]. Many urban forms or building designs have proven effective in improving the PLW environment, including wind passage[23], building height variation[3, 25], lower building packing density[6, 25, 26], building array arrangement[10, 27], arcade[28-30], and lift-up design[5, 31-35]. In lift-up buildings (also known as void decks or elevated buildings), the ground floor is replaced with supporting pillars or shear walls, and thus, an open space is formed for wind penetration into pedestrian areas. The benefits of lift-up design for weak wind conditions have been justified by a series of studies. Xia et al., through wind tunnel experiments, found that lift-up design can increase the downstream mean wind speed by ~3%–11%[32]. Du et al. conducted computational fluid dynamics (CFD) simulations to confirm the wind comfort improvement effects of lift-up design for “–,” “L,” “U,” and “□”-shaped buildings, which originated from the typical building configuration in a university campus[33]. The “–” -shaped building was the basic configuration, which comprised of a cuboid and two cylinders. The conducted water channel experiments indicated a double increase in PLW velocities in idealized urban street canyons after being modified with lift-up design[36, 37]. Although the surrounding buildings can adversely affect PLW comfort in the lift-up area, wind amplification is still observed[35]. Moreover, owing to ventilation improvement, lift-up design can improve pollutant dispersion[5, 38-40]. For high-density cities in tropical and subtropical climate zones, the shading effect of lift-up design is advantageous. Thermal comfort is the state of mind which expresses satisfaction with the thermal environment[41]. Wind speed and incident radiation are two important factors influencing thermal comfort. As expected, a lift-up building has better thermal comfort at the pedestrian level in the neighborhood than the corresponding normal building without lift-up design[9]. The open space underneath a lift-up building is thermally comfortable in the summer of Hong Kong[9, 42]. Du et al. further demonstrated that the lift-up area can serve as a cooling spot in summer, without becoming a cold site in winter[43].

As lift-up design gained more recognition, an increasing number of parametric studies started being conducted to enrich the knowledge of PLW comfort around and underneath lift-up buildings. The impacts of the lift-up core dimension, building dimension, corner modification, and incident wind direction on PLW comfort were systematically evaluated[31, 34, 44-46]. Furthermore, two multivariable optimization approaches were developed to determine the optimal PLW comfort around and beneath an isolated lift-up building[44, 45]. Du et al.[46] and Liu et al.[35] extended the PLW comfort study on an isolated building to that on building arrays, and further developed a multistage optimization method for determining the most desirable microenvironment for an idealized urban canyon with lift-up design[47]. Chew and Norford[36, 37] further identified the impacts of void deck height, building height, street aspect ratio, and building height variation on the PLW environment in idealized urban street canyons with void decks. Moreover, although the mean wind velocity gained maximum attention, the gust wind velocity around lift-up buildings was also investigated[35, 48].

The aforementioned studies involved various influential parameters and provided insightful findings on PLW comfort around lift-up buildings; however, most of them utilized traditional rectangular- or square-plan building models. Nevertheless, modern buildings are not uniform but have various configurations. An advancement in construction materials and methods immensely inspires architects' creativity in unconventional building configurations. Some building configurations are adopted as aerodynamic treatments to detrimental wind effects[49, 50]. Table 1 enumerates some commercial properties and public housings in Hong Kong. These unconventional configurations exhibit unique aerodynamic performances, and thereby, have different effects on PLW comfort[50-52]. The findings derived from lift-up buildings with conventional configurations may be insufficient to represent those with unconventional configurations. However, PLW comfort on lift-up buildings with various unconventional configurations is yet to be systematically evaluated. This study thereby aims to fill this research gap. Here, 22 building configurations are selected and modified as test models according to the existing buildings in Hong Kong (Table 1). Each configuration is examined under several incident wind directions. CFD simulations are utilized to reproduce the flow field around the buildings, whose accuracy is first validated using wind tunnel data. A comparative analysis between lift-up and normal buildings is conducted to investigate the impacts of lift-up design on PLW comfort under different configurations. Some configuration parameters are identified for further evaluating the influence of the performance of lift-up design. Specifically, the mean wind velocity is more representative for depicting the actual wind environment of interest precinct than the gust wind velocity, which is commonly measured for 2–3 s, especially under weak wind conditions[53]. Therefore, this study only concerns the mean wind velocity at the pedestrian level. It focuses on PLW comfort around lift-up buildings with unconventional configurations, which can provide a more comprehensive understanding of lift-up design's performance for improving PLW comfort for city planners and architects.

The rest of this manuscript is organized as follows. A validation study of the adopted CFD simulations is presented in Section 2. Section 3 draws a detailed description of the 22 building configurations and incident wind directions. Then, Section 4 presents the simulation results of PLW comfort around the lift-up buildings. A quantitative analysis is conducted to examine the effects of configuration parameters on PLW comfort and the performance of lift-up design. Some limitations of this study are discussed in Section 5. Finally, Section 6 concludes the study.

Table 1. Some commercial properties and public housings in Hong Kong, China (snapshotted from Google earth).

<table>
<tr><th colspan="4">(a) Polygonal buildings</th></tr>
<tr><td>
Bank of China Tower</td><td>
Cambridge House</td><td>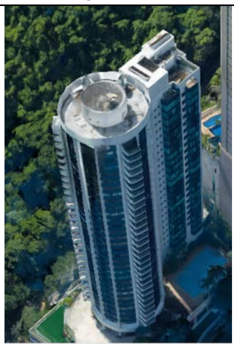
Century Tower</td><td>
Windsor House</td></tr>
<tr><th colspan="4">(b) Cruciform buildings</th></tr>
<tr><td>
Tsz Lok estate</td><td>
Merry court</td><td>
Faber Garden</td><td>
Tsz Oi Court</td></tr>
<tr><th colspan="4">(c) Slab-like buildings</th></tr>
</table>

 **Fung Tak estate**	 **Greenery Garden**
(d) Trident buildings	
 **Scenic Villa**	 **Mount Trio Court**
(e) Assembled buildings	
 **Tung tau estate**	 **Chak On Estate**

Nomenclature

PLW	Pedestrian-level wind
H, W, D	Height, width, and depth of building
d, h	Length and height of lift-up core
U	Mean wind velocity
U_{ref}	Reference wind velocity at the height of 150 m in the prototype scale
I	Turbulence intensity

Re	Reynolds number
υ	Kinetic viscosity coefficient
u^*	Frictional velocity
z_0	Dynamic roughness height
κ	Von Karman constant (κ = 0.4187)
k, ε	Turbulence kinetic energy and turbulence dissipation rate
C_μ	Model constant (C_μ= 0.09)
k_s, C_s	Roughness height and roughness constant
x, y, z	Stream-wise, lateral or span-wise, vertical directions
SRANS	Steady Reynolds-averaged Navier-Stokes
R	Correlation coefficient
NMSE	Normalized mean square error
FAC2	Fraction of predictions within a factor of two of observation
N	Number of sides
θ	Incident wind direction
α	Interior angle of equilateral polygonal models
slab-90, slab-120	Slab-like models with included angles of 90° and 120°
slab-135, slab-150	Slab-like models with included angles of 135° and 150°
crcfrm, crcfrm-A	Basic cruciform model, A-type cruciform model
crcfrm-B, crcfrm-C	B-type cruciform model, C-type cruciform model
trgl, rctglr, sqr, trpzd,	Triangular, rectangular, square, and trapezoidal models
pntgn, hxgn, octgn, crcl	Pentagonal, hexagonal, octagonal, and circular models
L	Linear model
MVR	Mean wind velocity ratio
MVR_DEF	Difference between *MVR* values of normal and lift-up buildings
MVR_{LFT}	*MVR* values around the lift-up and normal buildings
MVR_{NB}	*MVR* values around the normal buildings

K_{200}	Ratio of threshold wind velocity to reference mean wind velocity
UFWC	Unfavorable wind comfort
AWC	Acceptable wind comfort
UAWC	Unacceptable wind comfort
LWV	Low wind velocity
MWV	Moderate wind velocity
HWV	High wind velocity
DWV	Dangerous wind velocity
AR_C	Area ratio of the target wind comfort zone
C	Category of the target wind comfort zone
A_C, A_T	Areas of the target wind comfort zone and the selected research region
AR_{UFWC}	Area ratio of the unfavorable wind comfort zone
AR_{HWV}	Area ratios of the high wind velocity zone
AR_{AWC}	Area ratio of the acceptable wind comfort zone
ΔAR_C	Difference in AR_C between normal and lift-up buildings
AR_{NB}	AR_C in the case of normal building
AR_{LFT}	AR_C in the case of lift-up building
ΔAR_{UFWC}	Difference in AR_{UFWC} between normal and lift-up buildings
P_i	Occurrence probability
LES	Large eddy simulation

2. Validation of CFD simulations

2.1. Description of wind tunnel experiments

The wind tunnel experiments conducted by Xia et al.[32] were adopted in this study to validate the accuracy of CFD simulations in predicting the mean flow field at the pedestrian level around an isolated building with and without lift-up design. The experiments were accomplished in the CLP Power Wind/Wave Tunnel Facility (width × height × length: 3 m × 2 m × 29 m) at the Hong Kong University of Science and Technology. Fig. 1(a) presents the geometric dimensions in the prototype scale of two building models—normal building and lift-up building, each having dimensions of 50 m height (*H*), 75 m width (*W*), and 25 m depth (*D*). The lift-up building was lifted off the ground by three central supporting pillars, each of which had the same dimensions: 8 m (*d*) × 8 m (*d*) × 3.5 m (*h*); the spacing between the adjacent pillars was 17.5 m. The approaching wind was perpendicular to the windward plane of the building. Thus, the streamwise, lateral, and vertical directions were along the *x*-, *y*-, and *z*-coordinate axes, respectively. The origin coordinate was located at the center of the building's bottom plane. The blockage ratio was an important index for assessing the lateral-wall effects of wind tunnel experiments, which was defined as the projected area of building models divided by the cross-sectional area of the wind tunnel. The blockage ratio of the lift-up building model was ~1.6%, which was below the reference threshold value of 3%[54]. The pedestrian level was set as 2 m ($z = 0.04H$) off the ground, where all measuring sensors were installed. Before being placed in the wind tunnel, the two building models were scaled at a ratio of 1:200. Ai et al.[55] demonstrated that reduced-scale models in CFD simulations of wind-related issues can save considerable computation resources without degrading the prediction accuracy. Accordingly, the numerical simulation models had the same scales as the wind-tunnel models. The measurement data on three horizontal lines ($x = -0.25H$, $x = 2H$, and $x = 3.25H$) at the pedestrian level (Fig. 1(b)) were utilized to validate the CFD simulation results. Fig. 1(c) shows the vertical profiles of the normalized mean wind velocity ($U(z)/U_{ref}$) and turbulence intensity $I(z)$ profiles for the approaching flow[32], where U_{ref} denotes the mean wind velocity at a reference height of 150 m in the prototype scale, whose measured value in the wind tunnel was ~10 m/s. The approaching flow velocity was ~8.2 m/s at the building height; thus, the reference Reynolds number ($Re = \frac{UH}{\upsilon}$, where *H* is the characteristic height of the building and υ is the kinetic viscosity coefficient) equaled ~14×10^4. The *Re* value exceeded the threshold value of 1.5×10^4, ensuring that the flow field met the *Re*-independent similarity standard[55]. More detailed information about the wind tunnel experiments can be obtained from the literature[32, 33, 48].

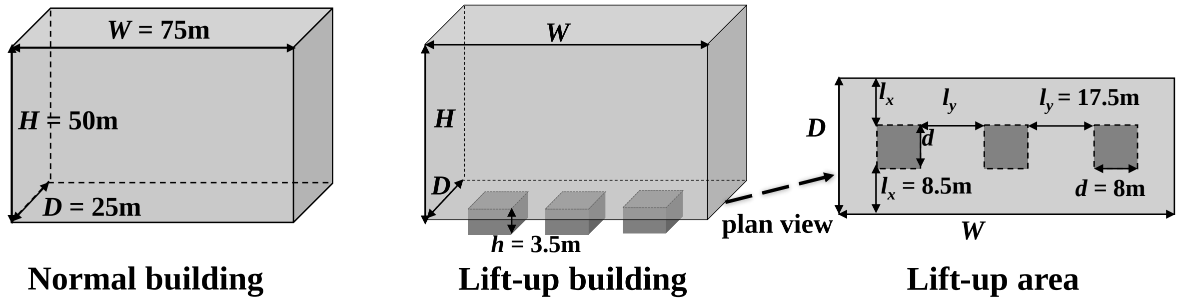
W = 75m
H = 50m
D = 25m
Normal building
W
H
D
h = 3.5m
Lift-up building
plan view
D
l_x
l_y
l_y = 17.5m
d
l_x = 8.5m
d = 8m
W
Lift-up area

(a)

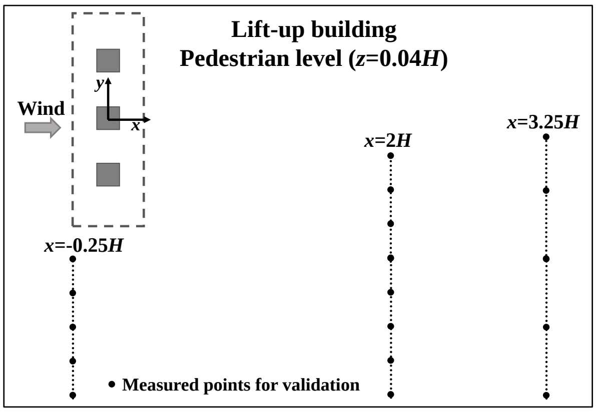
Lift-up building
Pedestrian level (z=0.04H)
Wind
y
x
x=2H
x=3.25H
x=-0.25H
Measured points for validation

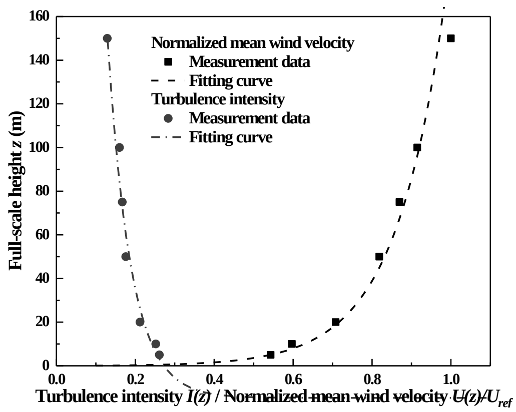
Normalized mean wind velocity
Measurement data
Fitting curve
Turbulence intensity
Measurement data
Fitting curve
Full-scale height z (m)
Turbulence intensity I(z) / Normalized mean wind velocity U(z)/U_{ref}

(b) (c)

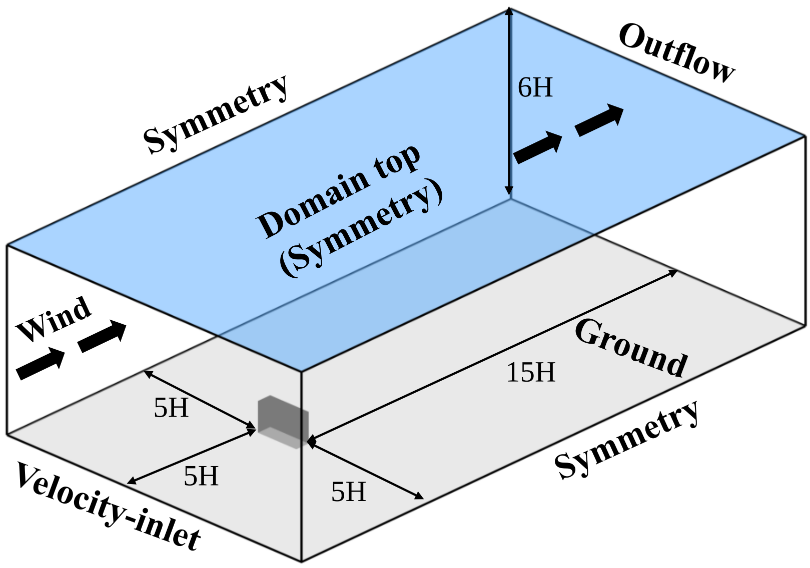
Symmetry
Outflow
6H
Domain top
(Symmetry)
Wind
Ground
15H
5H
5H
5H
Symmetry
Velocity-inlet

(d)

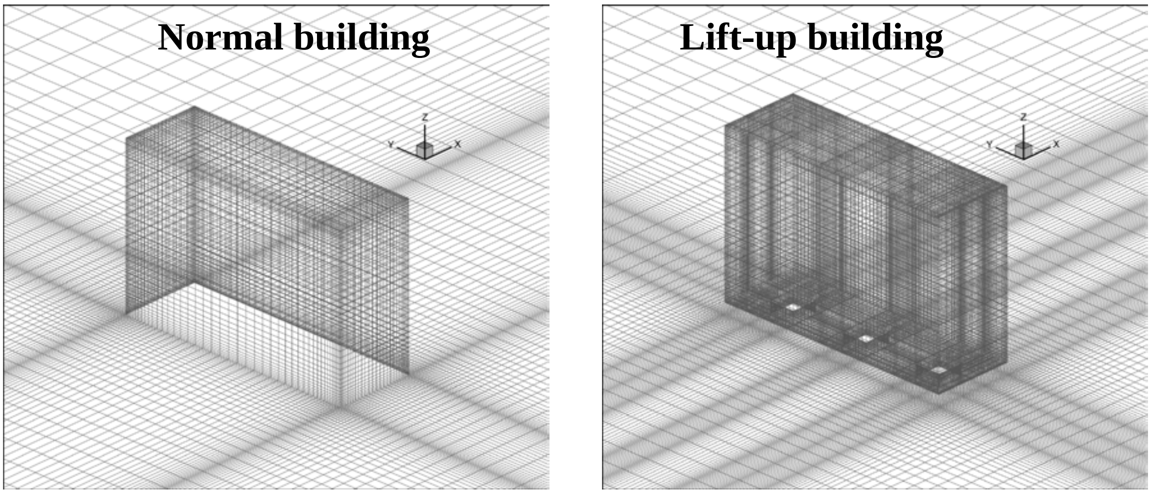

(e)

Fig. 1. (a) Geometric dimensions of normal and lift-up building models in the prototype scale, (b) schematic of measured points for validation (lift-up building as an example), (c) vertical profiles of normalized mean wind velocity and turbulence intensity for the approaching flow, and (d) computational domain, and (e) medium grid arrangements for normal and lift-up buildings.

2.2. Computational settings and parameters

The size and discretization of the computational domain were referred from the best practice guidelines[54, 57, 58]. The distances between the building and the inlet boundary, lateral boundaries, top boundary, and outflow boundary were 5H, 5H, 5H, and 15H, respectively, as shown in Fig. 1(d). Thereby, the blockage ratio was ~2.2%. The domain was discretized with structured hexahedral grids. The maximum stretching ratio of adjacent grids was 1.17. Three grid arrangements were constructed to conduct the grid sensitivity test. The minimum grids for coarse, medium, and fine grid arrangements were 0.001, 0.002, and 0.004 m, respectively. The total elements for normal building model were 609, 322 (coarse grid), 1, 300, 536 (medium grid), and 2, 046, 618 (fine grid), respectively. The total elements for lift-up building model were 1, 010, 793 (coarse grid), 2, 146, 725(medium grid), and 3, 605, 321 (fine grid), respectively. Fig. 1(e) displays the medium grid arrangements for normal and lift-up buildings.

As shown in Fig. 1(c), the measured approaching wind profile can be interpolated into a log-law curve. Thus, the velocity-inlet boundary condition in the domain was prescribed by the fitting log-law profile (Eq. (1)). Thereinto, the frictional velocity (u^*) was 0.53 m/s, the dynamic roughness height (z_0) was 0.00035 m, and the von Karman constant (κ) was 0.4187. Note that the values of u^* and z_0 were obtained by fitting Eq. (1) with measured data. The turbulence intensity vertical profile was also obtained from fitting the wind-tunnel measurement data. Therefore, the turbulence kinetic energy (k) profile was determined by Eq. (2)[54]. By assuming a local equilibrium between the turbulence production and dissipation terms, the inlet profile of the turbulence dissipation rate (ε) can be described by Eq. (3)[54], where C_μ = 0.09 is the model constant. The ground and building surfaces were defined as the no-slip wall boundary. To minimize the horizontal inhomogeneity of the atmospheric boundary layer in the domain, the k_s-type wall function (Eq. (4))[59] was adopted for the ground surface, where k_s indicates the sand-grain roughness height and C_s indicates the roughness constant. In this paper, for the value of k_s to be less than the distance from the center of the wall-adjacent grid to the wall, k_s was set as 0.00045 m. The top and lateral sides of the domain were specified as symmetry boundaries, namely setting normal velocity and normal gradients of all variables to zero. The outflow boundary condition was adopted at the domain outlet as the domain downstream was long enough to ensure a fully developed outlet flow.

$$U(z) = \frac{u^*}{\kappa} \ln\left(\frac{z+z_0}{z_0}\right), \tag{1}$$

$$k(z) = \frac{3}{2}\left(I(z)U(z)\right)^2, \tag{2}$$

$$\varepsilon(z) = C_\mu^{\frac{1}{2}} k(z) \frac{dU(z)}{dz}, \tag{3}$$

$$k_s = \frac{9.793 z_0}{C_s}. \tag{4}$$

ANSYS Fluent 13.0[60] was used to perform the CFD simulations. Because this study only focused on the mean flow, steady Reynolds-averaged Navier-Stokes (SRANS) equations were adopted to predict the flow field to save the computational cost. According to the review papers on the application of CFD simulations to the wind environment, SRANS is the most widely used approach[61, 62]. The realizable k-ε turbulence model proposed by Shih et al.[63] was employed for the equation closure, which has proven sufficiently accurate and reliable in modeling the PLW environment[50, 64-71]. The SIMPLEC algorithm was selected for pressure–velocity coupling. Both convective and diffusive terms of the governing equations were discretized by the finite volume method with the second-order discretization scheme. The underrelaxation factors for the pressure, momentum, turbulent kinetic energy, and turbulent dissipation rate terms were set as 0.3, 0.7, 0.8, and 0.8, respectively. The iteration computation for all governing equations lasted until the residual curves were approximately stable and the residuals were below 10^{-4}. Specifically, the convergence residuals were below 10^{-4} for the continuity equation, 10^{-6} for the momentum and k equations, and 10^{-5} for the ε equation.

2.3. Validation study

Fig. 2 presents three horizontal profiles (x = -0.25H, x = 2H, and x = 3.25H) of the normalized mean wind velocity ($U(z)/U_{ref}$) around the normal and lift-up buildings at the pedestrian level (z = 0.04H). The results indicated that the simulated profiles matched the wind-tunnel data well at most of the measured positions. A distinct underestimation mainly occurred in the wake region (x = 2H and x = 3.25H), which is an intrinsic deficiency of the SRANS approach due to its incapability of reproducing vortex shedding in the wake region[61, 62, 65, 72]. In addition, the discrepancy of the simulated profiles between medium and fine grid arrangements was negligible, indicating that the medium grid arrangement is sufficiently suitable for obtaining a stable flow regime independent of the grid systems. To quantify the accuracy of the employed CFD model, four statistical metrics were calculated using wind-tunnel data and simulation results from medium grid arrangement, namely the correlation coefficient (R), the fraction bias (FB), the normalized mean square error (NMSE), and the fraction of predictions within a factor of two of observation (FAC2). According to the literature[73-75], the statistical performance metrics for a good prediction should meet the following criteria: R > 0.8, |FB| < 0.3, NMSE < 4, and FAC2 > 0.5. As presented in Table 2, for lift-up building models, the employed CFD model tends to underestimate the mean wind velocity (FB > 0). For normal building models, the underestimation is also observed at x = -0.25 H and 3.25H (FB > 0) except at x = 2 H (FB < 0). Nevertheless, the discrepancy is acceptable as the values of NMSE (0 – 0.31) and FB (-0.062 – 0.068) are small. Overall, because the values of R, FB, NMSE, and FAC2 are all within the recommended criteria, it can be concluded that the employed CFD model could predict the mean flow field with satisfactory accuracy.

As the minimum grid resolution of the medium grid arrangement was 0.002 m, the average value of near-wall y^+ for the building surface and domain ground was ~30. Furthermore, there were four to five grid layers below the pedestrian level. Consequently, the SRANS approach with a realizable k-ε turbulence model, standard wall function and medium grid arrangement could predict PLW flow fields around both normal and lift-up buildings with acceptable accuracy and economical computation cost.

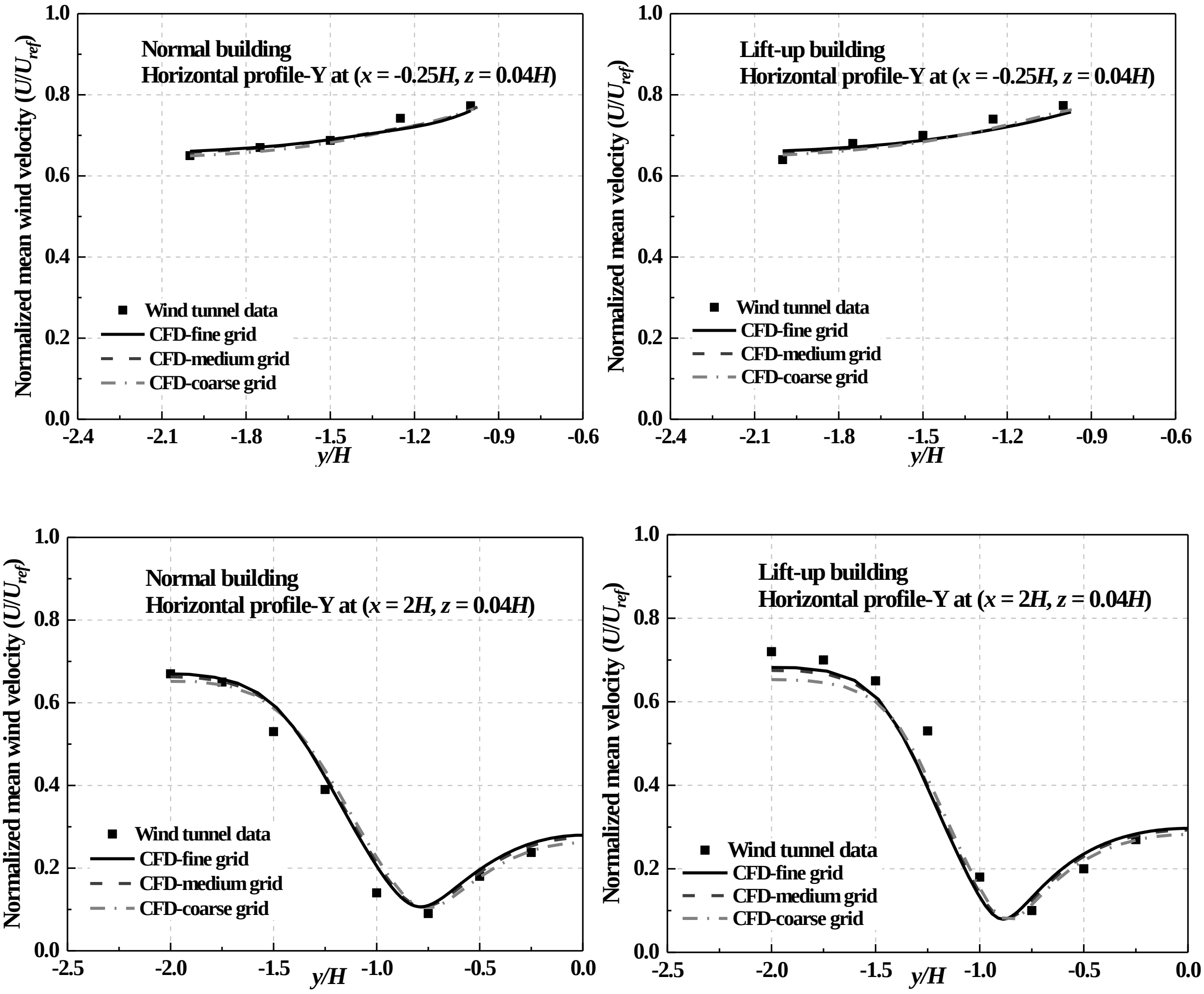

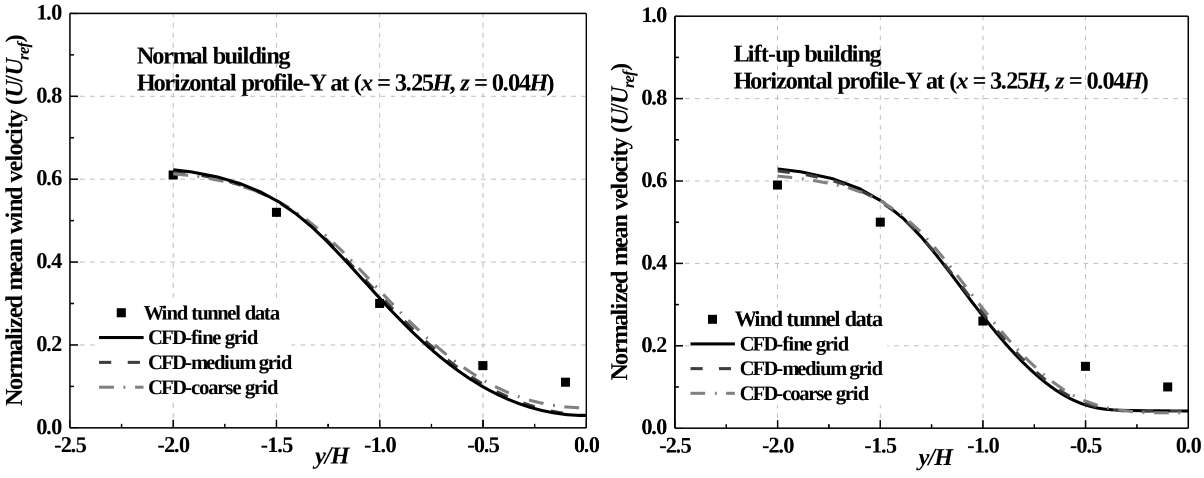

(a) Normal building model (b) Lift-up building model

Fig. 2. Comparison of wind-tunnel and CFD simulated $U(z)/U_{ref}$ at the pedestrian level (z = 0.04H): (a) normal building model, (b) lift-up building model.

Table 2. Summary of validation metrics for $U(z)/U_{ref}$ values.

	Normal building (Fig. 2(a))			Lift-up building (Fig. 2(b))		
	x = -0.25H	x = 2H	x = 3.25H	x = -0.25H	x = 2H	x = 3.25H
R	0.989	0.994	0.995	0.971	0.984	0.993
FB	0.007	-0.062	0.045	0.015	0.068	0.027
NMSE	0.0003	0.008	0.016	0.0007	0.019	0.031
FAC2	1	1	1	1	1	0.6

3. Description of tested configurations

3.1. Case arrangement

As shown in Table 3, 22 building configurations were studied, which were classified into five groups: “polygonal,” “slab-like,” “cruciform,” “trident,” and “assembled.” Each configuration had two building forms: normal building without lift-up design and lift-up building. Thus, there were 22 normal and 22 lift-up building models, all of which were 50 m high (H) in the prototype scale. The lift-up buildings were directly elevated off the ground without any pillar. The lift-up height (h) was 3.5 m in the prototype scale. The lift-up core dimension proved to influence the PLW comfort around/underneath the building[31, 34, 43]. The core structure was thereby omitted, as the research focus was building configuration. Such simplification of the lift-up design has been accepted previously[5, 36, 37]. The basic plan area for the building models was set as 1344 m^2, based on the typical floor plan of Hong Kong public rental housing estates[72]. The plan area deviation among different configurations was within 2%. All building models, except for a few special ones, were tested under three typical wind directions (θ). The detailed information regarding this is given in the following paragraphs.

The polygonal models included triangular, quadrangular, pentagonal, hexagonal, octagonal, and circular models, which were abbreviated to "trgl," "rctglr," "sqr," "trpzd," "pntgn," "hxgn," "octgn," and "crcl," respectively. Each polygonal model was equilateral, except for the quadrangular models, which included three plan forms of square, rectangle, and trapezoid. These equilateral models' interior angles (α) were 60°, 90°, 108°, 120°, 135°, and 180°, respectively. Considering the axial symmetry law of a regular polygon, the tested wind directions were set as 0°, 0.5× (180° - α), and 0.25× (180° - α), successively. For instance, three typical wind directions for the square model were 0°, 22.5°, and 45°. Note that the circular model only had one tested wind direction, which was perpendicular to the windward surface. The rectangular model was tested under $\theta = 0°$, 45°, and 90°, while the trapezoidal model was tested under an additional wind direction of 180°.

Slab-like models comprised two symmetric identical slabs, including slab-90, slab-120, slab-135, and slab-150, with included angles of 90°, 120°, 135°, and 150°, respectively. The arc-150 model was one-sixth of a circular ring, designed as a contrast case of slab-150 model. Studies conducted on the passage flow between two nonparallel buildings indicated that the converging and diverging flows exhibited quite different flow patterns[67, 77-79]. Similarly, the distinction between the converging flow ($\theta = 0°$) and diverging flow ($\theta = 180°$) was investigated in this study. Hence, three typical wind directions were set as 0°, 90°, and 180°.

The cruciform model and its variants are widely used in residential blocks. In this study, the following four types were selected: "crcfrm," "crcfrm-A," "crcfrm-B," and "crcfrm-C." The crcfrm model was the basic one, and comprised rectangular-plan blocks; its configuration referred to the standard block typical floor plan of Hong Kong[72]. The crcfm-A model had a cavity in the center of each extended part, making the surface more uneven. In the crcfm-B model, eight sharp corners were modified to the recessed corners. As for the crcfm-C model, the right-angle notches were padded to be flatter. These models were tested at $\theta = 0°$, 22.5°, and 45°.

Trident and assembled models are also common configurations for public rental housing estates of Hong Kong[72]. The Y model can be regarded as a variant of model slab-120, in which all three included angles are 120°. In the T model, three obtuse angles are converted into two right angles and one straight angle. The tested wind directions for the trident models were thereby set consistently with slab-like models. H, I, and linear (L) models were assembled by two or three rectangular models, with tested wind directions of 0°, 22.5°, and 45°.

Table 3. Geometric information regarding the tested building configurations in the prototype scale.

Type	(a) Polygonal models							
Configurations of floor plan	Triangular "trgl"	Quadrangular Rectangular "rctglr"	Square "sqr"	Trapezoidal "trpzd"	Pentagonal "pntgn"	Hexagonal "hxgn"	Octagonal "octgn"	Circular "crcl"
Schematic	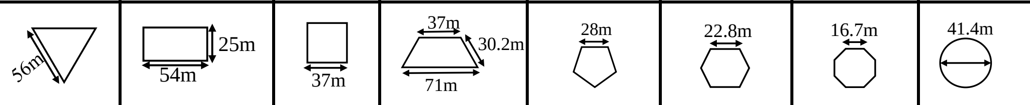							
Number of sides N	3	4	4	4	5	6	8	Infinite
Plan area (m^2)	1358	1350	1369	1350	1349	1351	1347	1346
Interior angle α (°)	60	90	90	124.2/55.8	108	120	135	180
Wind direction θ (°)	0, 30, 60	0, 45, 90	0, 22.5, 45	0, 45, 90, 180	0, 18, 36	0, 15, 30	0, 11.5, 22.5	0
Definition of θ	$\theta = 0°$ ⬇		$\theta = 45°$ ⬊			$\theta = 90°$ ➡		⬆ $\theta = 180°$

Type	(b) Slab-like models				
Configurations of floor plan	slab-90	slab-120	slab-135	slab-150	arc-150
Schematic	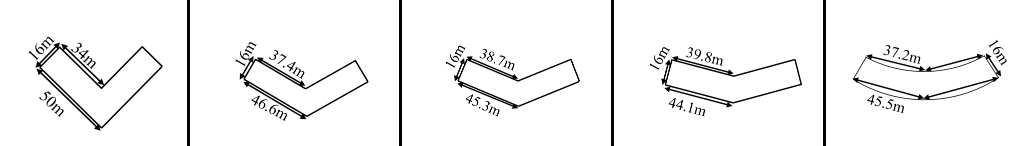				
Plan area (m^2)	1344	1344	1344	1342.4	1340.4
Included angle	90	120	135	150	150

α (°)					
Wind direction θ (°)	0, 90, 180	0, 90, 180	0, 90, 180	0, 90, 180	0, 90, 180
Definition of θ	$\theta = 0°$ Converging flow		$\theta = 90°$		$\theta = 180°$ Diverging flow
Type	(c) Cruciform models				
Configurations of floor plan	crcfrm	crcfrm-A	crcfrm-B	crcfrm-C	
Schematic	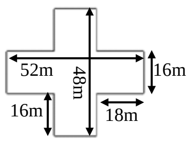	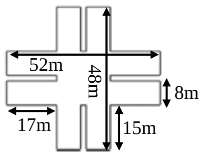	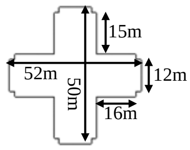	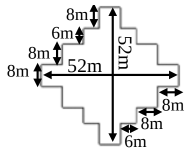	
Plan area (m²)	1344	1344	1344	1360	
Wind direction θ (°)	0, 22.5, 45	0, 22.5, 45	0, 22.5, 45	0, 22.5, 45	
Definition of θ	$\theta = 0°$		$\theta = 22.5°$	$\theta = 45°$	
Type	(d) Trident models		(e) Assembled models		
Configurations of floor plan	Y	T	H	I	Linear "L"
Schematic	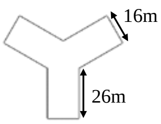	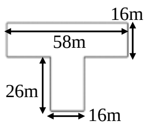	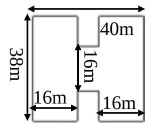	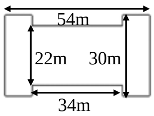	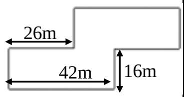
Plan area (m²)	1359	1344	1344	1348	1344
Wind direction θ (°)	0, 90, 180	0, 90, 180	0, 45, 90	0, 45, 90	0, 45, 90
Definition of θ	$\theta = 0°$	$\theta = 45°$		$\theta = 90°$	$\theta = 180°$

3.2. Computational settings and parameters

Similar to the modeling approach described in Section 2, all building models in CFD simulations were scaled by 200 to the prototype sizes, which was consistent with the validation tests in order to save computation resources. The computational domain size was set similarly to that in the validation cases in Section 2. The maximum blockage ratio of the domain among all cases was ~2.4%, which is less than the maximum acceptable value of 3%[53]. The computational domain was discretized into structured hexahedral cells (e.g. Fig.3) with a minimum resolution of 0.002 m. The total number of hexahedral cells for each case ranged from ~1.4 million to 3.2 million. All cases were computed with the same inflow wind profiles and boundary conditions of validation cases. Furthermore, the turbulence model, discretization method, wall function, solution scheme, and convergence criterion used for all cases were in accordance with the settings of the validation cases.

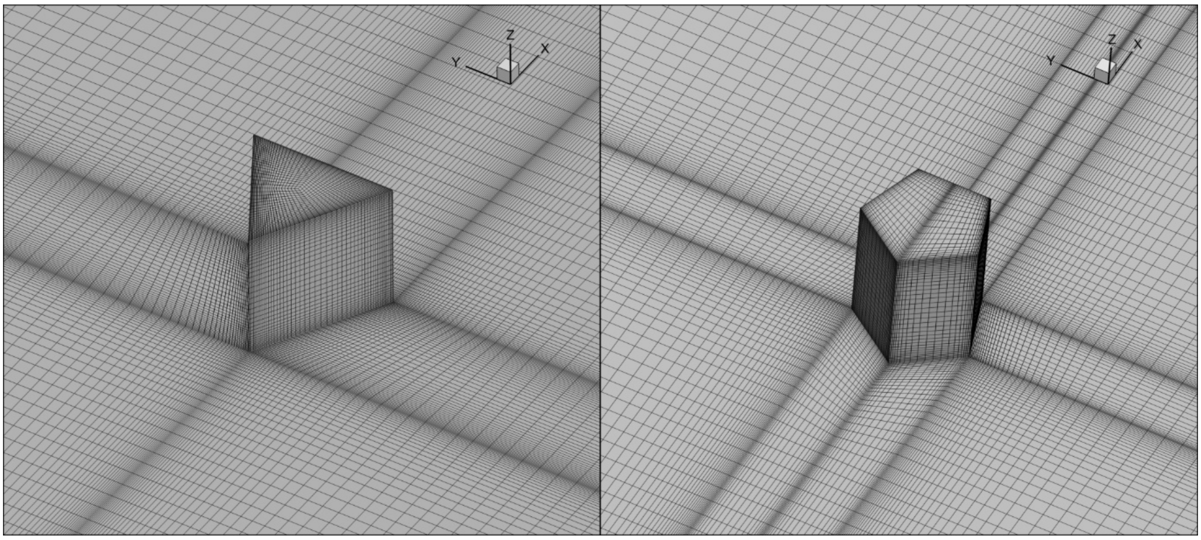

Fig. 3. Mesh arrangements for triangular and pentagonal models.

4. Results

4.1. Wind parameters and wind comfort criterion

The mean wind velocity ratio (*MVR*) is adopted as a wind parameter to indicate the PLW comfort. It is defined as the ratio of mean wind velocity (U) of interest points at the pedestrian level to the mean wind velocity (U_{ref}) of the inlet flow at the reference height without any influence of the urban blocks (Eq. (5))[23]. In this paper, the reference height is assumed to be 4H[48, 80], namely 1 m, corresponding to 200 m in the prototype scale[33, 34, 43, 45]. Specifically, according to the inlet wind velocity profile, the value of U_{ref} is 10 m/s. Besides, *MVR_DEF* is employed to quantitatively evaluate the effects of lift-up design on PLW comfort[33]. It represents the difference between the mean wind velocity fields of normal and lift-up buildings. As shown in Eq. (6), MVR_{LFT} and MVR_{NB} denote *MVR* values at the same position around the lift-up and normal buildings, respectively.

$$MVR = \frac{U}{U_{ref}} \tag{5}$$

$$MVR\_DEF = \frac{MVR_{LFT} - MVR_{NB}}{MVR_{NB}} \tag{6}$$

Recently, a series of PLW criteria applicable to either strong or weak wind conditions have been proposed. As this study concerns PLW comfort under weak wind conditions, two wind comfort criteria [1, 34] (shown in Table 4(a–b)) suitable for weak wind conditions of Hong Kong are adopted as references. They accept the comparable threshold values for low wind velocity (1.5–1.6 m/s) and unacceptable wind velocity (5–5.3 m/s). The long-term mean wind velocity measured at a reference height of 200 m over Hong Kong is ~5 m/s, with a 50% probability of exceedance[1, 33, 34]. Thus, when the value of *MVR* falls between 0.3 and 1.06, the PLW comfort is identified as acceptable; otherwise, it is considered unfavorable (*MVR* < 0.3) or unacceptable (*MVR* > 1.06). Although the gentle breeze (3.5–5.3 m/s) begins to disorder hair and flap clothing[81, 82], it is still acceptable for the pedestrians. On this basis, a value of *MVR* between 0.7 and 1.06 is defined as high wind velocity, while that between 0.3 and 0.7 is referred as moderate wind velocity. Table 4(c) provides a detailed description of the wind comfort criterion adopted in this study.

Table 4. Novel PLW comfort criteria for weak wind conditions of Hong Kong.

(a) Wind comfort criterion proposed by Du et al.[1]

Category	**Threshold wind velocity**	***MVR***	**Remarks**
Unfavorable	<1.5	<0.3	N/A
Acceptable	<1.8	<0.36	Sitting long
	<3.6	<0.72	Sitting short
	<5.3	<1.06	Strolling
Tolerable	<7.6	<1.52	Walking fast
Intolerable	>7.6	>1.52	Not suitable for activities
Dangerous	>15	>3	Dangerous

(b) Wind comfort criterion proposed by Zhang et al.[34]

Category	**Threshold wind velocity**	***K_{200}***	**Remarks**
Low wind speed	<1.6	<0.3	***K_{200}*** is the ratio of threshold wind velocity to reference mean wind velocity (5 m/s) at 200 m height.
Acceptable	1.6–3.5	0.3–1	
High wind speed	3.5–5	0.7–1	
Unacceptable	>5	>1	

(c) Wind comfort criterion used in this study

Category	**Threshold wind velocity**	***MVR***	**Remarks**
Unfavorable wind comfort (UFWC)	<1.5	<0.3	Low wind velocity (LWV)
Acceptable wind comfort (AWC)	1.5–3.5	0.3–0.7	Moderate wind velocity (MWV)
	3.5–5.3	0.7–1.06	High wind velocity (HWV)
Unacceptable wind comfort (UAWC)	>5.3	>1.06	Dangerous wind velocity (DWV)

4.2. General flow characteristics in the surrounding of lift-up buildings

As shown in Fig. 4, cases of square model at $\theta = 0°$ are taken as examples to demonstrate the general flow characteristics at the pedestrian level around normal and lift-up buildings. The coordinate axis is normalized with respect to the building height *H*. Similar to[33, 34], three typical wind comfort zones—upstream unfavorable wind comfort zone (*MVR* < 0.3), downstream unfavorable wind comfort zone, and lateral high wind velocity zone (0.7 < *MVR* ⩽ 1.06)—are generated due to the blocking effect around both normal (Fig. 4(a)) and lift-up buildings (Fig. 4(b)). However, no unacceptable wind comfort zone (1.06 < *MVR*) is found. The lateral high wind velocity zone is where the corner stream is located. The open space underneath the lift-up building provides a wind passage for streamwise and downward flows passing through, varying the surrounding wind comfort zones' magnitude and area. The confluence of throughflow and return flow results in low wind velocities in the downstream near field of the lift-up building. Clearly, the throughflow is moderated along the penetration depth.

The difference in *MVR* values between the normal and lift-up buildings (i.e., *MVR_DEF*) is illustrated in Fig. 4(c). The positive values (red contour) indicate the mean wind velocities amplified by the lift-up design, while the negative values (blue contour) indicate those impaired by the lift-up design. Compared to the normal buildings, the upstream, lateral, and downstream wind comforts near the lift-up buildings are increased by more than 20%. However, there are conspicuous *MVR* reduction zones in the downstream, which means that the lift-up design can degrade the PLW comfort in some downstream areas. This is because the throughflow provides a "cushion" in the cavity zone and slows down the wind flow recovery to the upstream undisturbed flow[48]. In addition, the effects of lift-up design vary with the distance to the building. Therefore, as shown in Fig. 4(c), four research regions with different scopes are defined to more precisely assess the lift-up design's performance. Region XS is the inner layer around the target building with dimensions of $2H \times 2H$, sequentially embraced by Region S ($4H \times 4H$), Region M ($6H \times 6H$), and Region L ($14H \times 6H$). Specifically, Region XS refers to the near field of the building and Region L refers to the full field of the building.

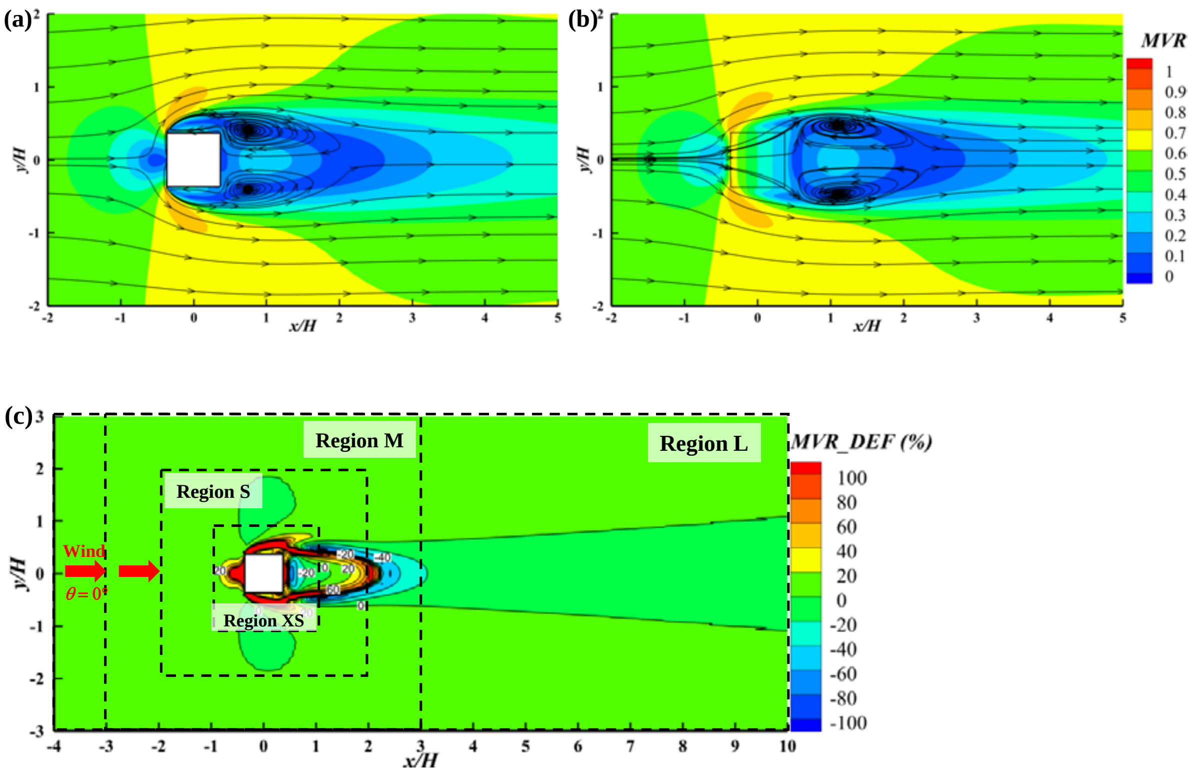

Fig. 4. Distribution of pedestrian-level *MVR* and streamlines for square model at $\theta = 0°$: (a) normal building, (b) lift-up building, (c) *MVR_DEF* contour.

4.3. The effects of lift-up design on PLW comfort (ΔAR_{UFWC})

To quantify the size of wind comfort zones around differently shaped buildings, the area ratio (AR_C) of the target wind comfort zone is defined as

$$AR_C = \frac{A_C}{A_T} \tag{7}$$

where subscript C indicates the category of the target wind comfort zone. Thus, A_C is the area of the target wind comfort zone and A_T is the total area of the selected research region. For instance, when calculating the area ratio of an unfavorable wind comfort zone (AR_{UFWC}) in Region XS, A_{UFWC} is the area of the unfavorable wind comfort zone in Region XS and A_T is its total area (i.e., $2H \times 2H$). Particularly, the lift-up area is excluded from the calculation of A_C. Obviously, the lesser the value of AR_{UFWC}, or the greater the value of AR_{AWC}, the better is the PLW comfort. Furthermore, the difference in the area ratio between normal and lift-up buildings (ΔAR_C) is used to assess the comprehensive effectiveness of the lift-up design, which can be calculated as

$$\Delta AR_C = \frac{AR_{LFT} - AR_{NB}}{AR_{NB}} \tag{8}$$

where the subscripts *LFT* and *NB* represent the cases of lift-up and normal buildings, respectively.

4.3.1. Variation of ΔAR_{UFWC} with incident wind direction and research region

Fig. 5 presents the values of ΔAR_{UFWC} between normal and lift-up buildings for all tested configurations. Although most configurations are tested under three typical wind directions, here only the maximum and minimum ΔAR_{UFWC} values among all tested wind directions are displayed. The corresponding wind directions are annotated near the values. The negative values indicate that the lift-up design improves the unfavorable wind comfort; otherwise, the positive values imply that the lift-up design worsens the unfavorable wind comfort. The differences between maximum and minimum ΔAR_{UFWC} values are pronounced in most cases, which indicates that the performance of the lift-up design is highly sensitive to the incident wind direction for most configurations. Furthermore, with wider size of the research regions, ΔAR_{UFWC} values show an increasing tendency. For individual models, such as slab-135 and slab-150, ΔAR_{UFWC} values in Region M are slightly greater than those in Region L. This is because the reduction in denominators between Regions M and L exceeds the decrement of numerators (Eq. (8)). In Region XS (Fig. 5(a)), all values are negative. In Regions S and M (Fig. 5(b–c)), the maximum values of some configurations are positive. In Region L (Fig. 5(d)), positive values even occur for minimum ΔAR_{UFWC}. This phenomenon reveals that the lift-up design can substantially improve the PLW comfort by up to 40%–70% in the near field of buildings. However, the wind comfort improvement weakens with the distance to the target building and may even reversely turn into an adverse effect.

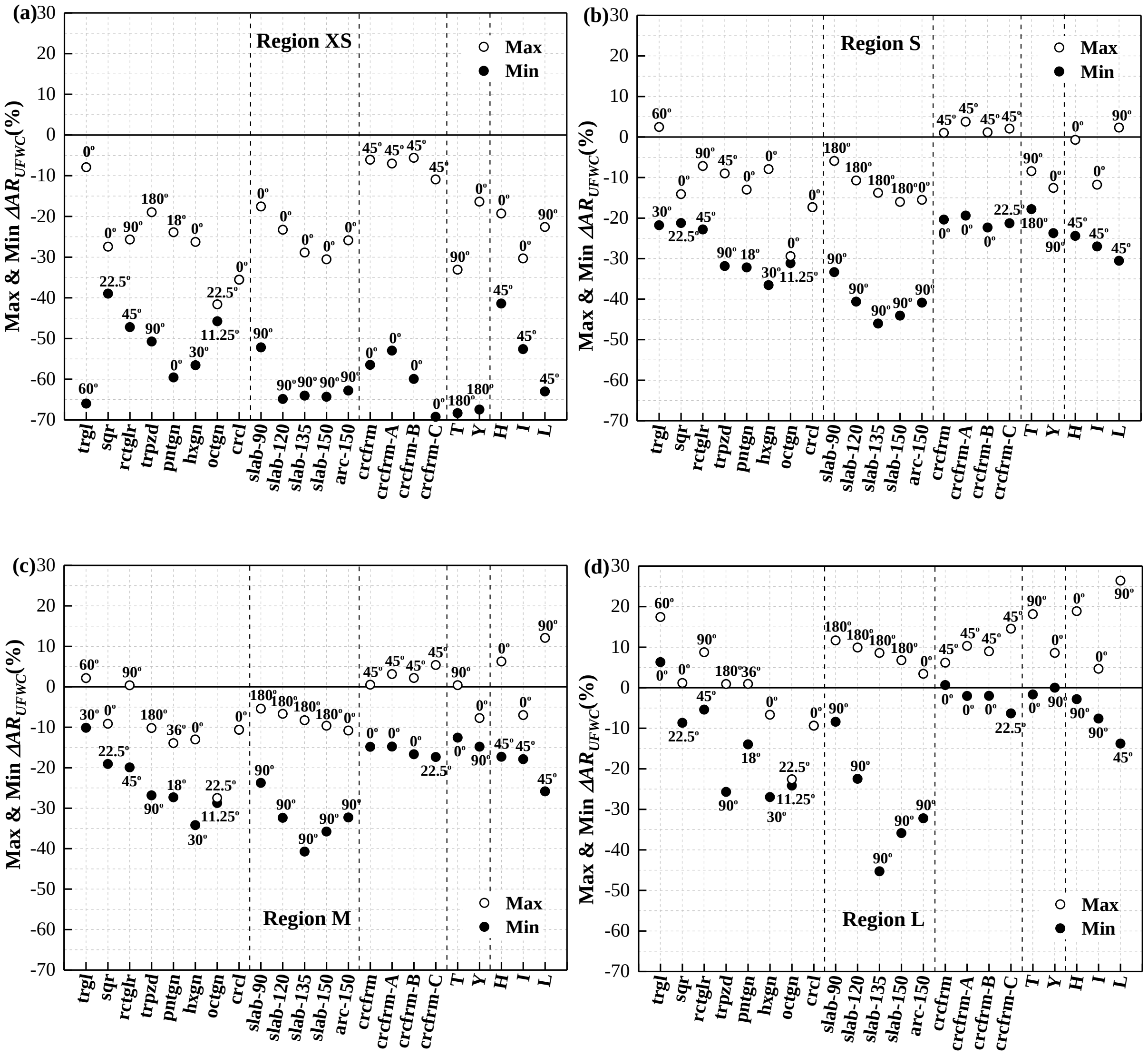

Fig. 5. Maximum and minimum ΔAR_{UFWC} values between normal and lift-up buildings in (a) Region XS, (b) Region S, (c) Region M, and (d) Region L.

4.3.2. Variation of full-field ΔAR_{UFWC} with building configuration

When the interest precinct is large (Fig. 5(d)), the performance of the lift-up design for PLW comfort varies with the building configurations. For instance, for triangular models, ΔAR_{UFWC} values of lift-up buildings in region L increase by 6%–17% compared to normal buildings. This indicates that although the lift-up design can improve the near-field wind comfort, it can concurrently enlarge the range of the unfavorable wind comfort zone in the far field. For hexagonal, octagonal, and circular models, the comprehensive effects of the lift-up design are always advantageous (Max and Min ΔAR_{UFWC} <0), shrinking the range of the unfavorable wind comfort zone. For the rest of the configurations, the minimum ΔAR_{UFWC} value is negative or near zero, whereas the maximum ΔAR_{UFWC} value is positive. Such phenomena suggest that the effect of the lift-up design is beneficial under some wind directions, but becomes detrimental or negligible under other wind directions.

4.3.3. Variation of near-field ΔAR_{UFWC} with building configuration

For polygonal and assembled models, the efficiency of lift-up design's effect on reducing the area of unfavorable wind comfort zone (ΔAR_{UFWC}) varies explicitly with configurations in the near field. For polygonal models, the values of maximum and minimum ΔAR_{UFWC} range from ~-36% to -66% and ~-8% to -42%, respectively. The changes of maximum and minimum ΔAR_{UFWC} among assembled models reach up to ~57% and ~52%, respectively. As for trident models, the maximum efficiency (minimum ΔAR_{UFWC}) of lift-up design changes little between Y and T models but the difference of maximum ΔAR_{UFWC} value between the two models is prominent.

For slab-like models, all minimum ΔAR_{UFWC} values are obtained from the case of $\theta = 90°$, indicating that the lift-up design has the most efficient performance at $\theta = 90°$. Although the change of minimum ΔAR_{UFWC} between slab-120 and slab-90 models is ~24%, the differences among slab-120, slab-135, slab-150, and arc-150 models are not significant. The maximum ΔAR_{UFWC} value in region XS is acquired at $\theta = 0°$. In terms of improving the near-field wind comfort, the lift-up design exhibits more efficiently under diverging flow ($\theta = 180°$) than under converging flow ($\theta = 0°$). Furthermore, under converging flow, the slab-150 has the greatest near-field ΔAR_{UFWC} value, which is ~74% greater than that of the slab-90 model. The findings suggest that lift-up design tends to perform more efficiently for slab-like building with a large included angle.

For cruciform models, all minimum near-field ΔAR_{UFWC} values are obtained at $\theta = 0°$, and all maximum near-field ΔAR_{UFWC} values are obtained at $\theta = 45°$. The results indicate that the lift-up design exhibits the most effective performance for wind comfort improvement at $\theta = 0°$ ($\Delta AR_{UFWC} < -50\%$). Moreover, the efficiency varies among four cruciform configurations, as evidence from the difference of ΔAR_{UFWC} between crcfrm-B and crcfrm-C models reaching ~31%. On the other hand, the lift-up design has insignificant effects on shrinking the unfavorable wind comfort zone at $\theta = 45°$ ($\Delta AR_{UFWC} > -11\%$).

Overall, there is no doubt that the lift-up design can efficiently decrease the area of unfavorable wind comfort zone and improve the PLW comfort in the near-field. However, the improvement efficiency is sensitive to the incident wind direction for most configurations and weakens with the size of the research region. Furthermore, the building configuration affects the performance of lift-up design to some extent.

4.4. PLW comfort around polygonal and assembled models (AR_{UFWC} and AR_{HWV})

4.4.1. Effects of number of sides (*N*)

Fig. 6(a) shows the maximum and minimum AR_{UFWC} values in Region XS among all tested wind directions for equilateral polygonal models. The case name is referred by the number of sides. The corresponding wind directions are annotated near the symbols. Apparently, the differences between the maximum and minimum AR_{UFWC} values are large for triangular and square models, which suggests that these configurations are sensitive to incident wind directions. With the number of sides increasing, the PLW comfort around the polygonal models becomes less sensitive to the wind direction.

To evaluate the integral performance of each configuration of PLW comfort under all wind directions, the mean AR_C is used as an indicator. It is the weight average of area ratios under all wind directions, and can be expressed as

$$\text{mean } AR_C = \sum_{i=1}^{n} AR_{C,i} \times P_i \tag{9}$$

where n is the number of tested wind directions, i is the specific incident wind direction, and P_i is the occurrence probability of the i wind direction. In this study, the occurrence probability of each typical wind direction for each model is assumed to be equivalent.

The mean AR_{UFWC} values for equilateral polygonal models in Region XS are presented in Fig. 6(b). In the near field, the mean AR_{UFWC} values decrease first (from N = 3 to N = 5 or 6) and then slightly increase with the number of sides. The change of mean AR_{UFWC} values is more pronounced among lift-up buildings than among normal buildings. For normal buildings, the triangular model (N = 3) has a 35.3% larger mean AR_{UFWC} value than the pentagonal model (N = 6). For lift-up buildings, the mean AR_{UFWC} value of the triangular model is a 70.2% increment of that for the hexagonal model (N = 5). As shown in Fig. 7(a), when expanding the interest precinct to Region L, the mean AR_{UFWC} values display a decreasing trend with the number of sides. The mean AR_{UFWC} value of lift-up triangular model is about 95% greater that of lift-up circular model. This indicates that circular buildings have the smallest area of the unfavorable wind comfort zone or the most desirable PLW environment, indicating that the circular cylinder or sphere has the least blocking effect on wind flow among the bluff bodies.

Fig. 7(b) shows the mean AR_{HWV} values for equilateral polygonal models in Region L. The mean AR_{HWV} values for lift-up buildings are greater than those for normal buildings. This implies that lift-up design can amplify the corner stream; this amplification is acceptable as no dangerous wind velocity (MVR > 1.06) occurs. When N varies from 3 to 5, the mean AR_{HWV} values show descending trends for both normal and lift-up buildings. Then, from N = 6, the values of lift-up buildings continue to decrease with the number of sides, while those of the normal buildings fluctuate by 0.1%.

The above results can provide good references for city planners when designing new constructions and determining the building orientation. When considering the full-field wind comfort, rounded configuration is the optimal choice; however, it does not perform well in the near-field wind comfort. If the dominant wind direction is monotonous and clearly known, triangular configuration with lift-up design can create the most comfortable PLW environment near the building under the condition of a favorable orientation. Nevertheless, if the local wind direction is fickle, pentagonal configuration with lift-up design exhibits the best comprehensive performance for near-field wind comfort.

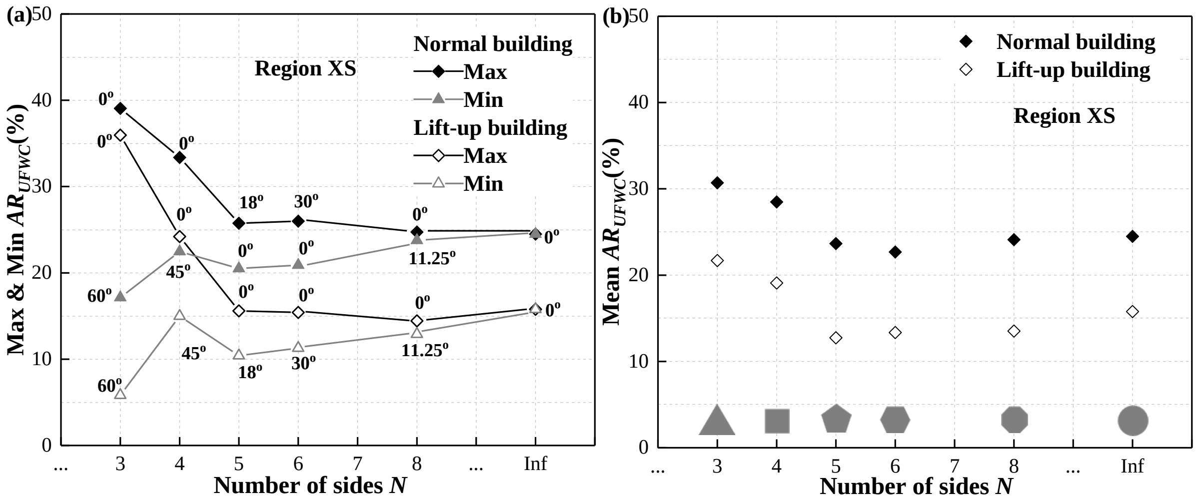

Fig. 6. (a) Maximum and minimum, (b) mean AR_{UFWC} values in Region XS among all wind directions for equilateral polygonal models.

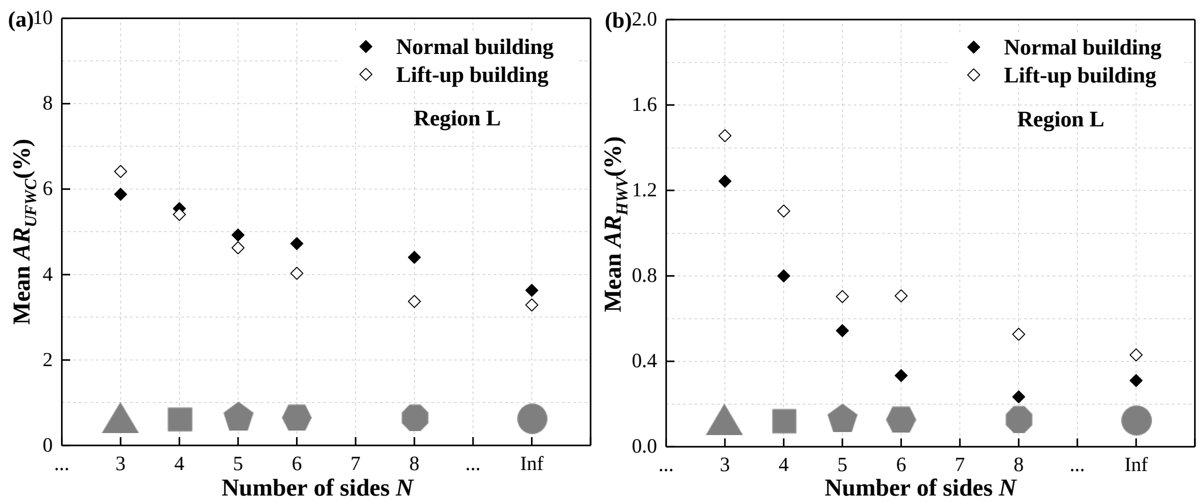

Fig. 7. Mean (a) AR_{UFWC} and (b) AR_{HWV} values in Region L for equilateral polygonal models.

4.4.2. Effects of projected width

The AR_{UFWC} and AR_{HWV} values of quadrangular building models (i.e. trapezoidal, rectangular, and square models) and assembled building models (i.e. H, I, and L models) in Region L under all tested wind directions are shown in Fig. 8, where "trpzd-180" denotes the trapezoidal models at $\theta = 180°$ and "H-0" refers to the H models at $\theta = 0°$; other models follow the same naming convention.

The projected widths of the trpzd-180, rctnglr-0, sqr-0, and rctnglr-90 models are 71, 54, 37, and 25 m in the prototype scale, respectively. As shown in Fig. 8(a), the AR_{UFWC} values (~11%, 9%, 6%, 3%) decline consistently with a reduction in the projected width of the building. As for assembled models, the projected widths of the H-0, I-0, and L-0 models in the prototype scale are 40, 54, and 68 m, respectively. The AR_{UFWC} values of these three models show an ascending tendency with the projected width increasing (Fig. 8(c)). The maximum increment among lift-up buildings can be ~56.8%. For the area of high wind velocity zone (AR_{HWV}), similar descending and ascending tendencies can be observed in Fig. 8(b, d), respectively. These results demonstrate that the projected width is an important factor for the areas of the unfavorable wind comfort zone and high wind velocity zone. Because the values of AR_{UFWC} and AR_{HWV} are normalized by the area of the full flow field, the variation magnitude looks small. More visualized information can be observed in Fig. 9, which depicts the contours of pedestrian-level *MVR* around lift-up trpzd-0, rctnglr-0, sqr-0, rctnglr-90, L-0, and H-0 models. From this figure, the area variations in the upstream and downstream unfavorable wind comfort zones and lateral high wind velocity zone with the projected width are distinct. The wide building tends to cause a greater area of unfavorable wind comfort zone and high wind velocity (corner stream) zone compared to the narrow one.

However, the projected width is not the only factor influencing the area of unfavorable wind comfort zone. The projected width of trpzd-0 model (71 m) is equal to that of trpzd-180 model (71 m), and greater than that of rctnglr-0 model (54 m). However, the AR_{UFWC} value of the trpzd-0 model (~8%) is smaller than those of both trpzd-180 (~11%) and rctnglr-0 models (~9%). The projected width (25 m) of trpzd-90 model is equal to that of rctnglr-90 model (~2.7%), but the trpzd-90 model has a half smaller AR_{UFWC} value (~1.3%). These findings suggest that the building depth (parallel to the incident wind) and the windward surface width may also influence the PLW comfort.

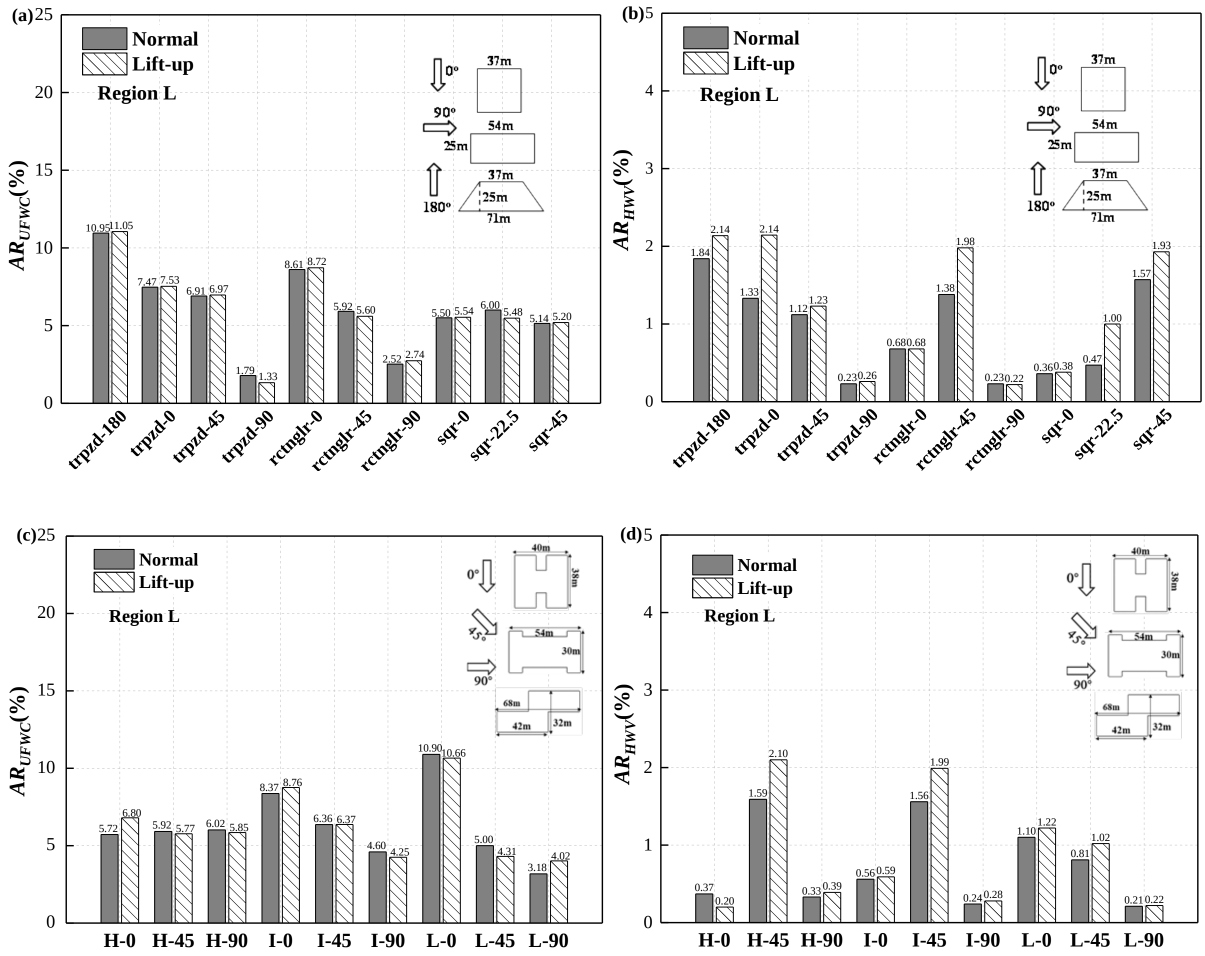

Fig. 8. (a) AR_{UFWC} and (b) AR_{HWV} values of quadrangular models, (c) AR_{UFWC} and (d) AR_{HWV} values of assembled building models in Region L under all tested wind directions.

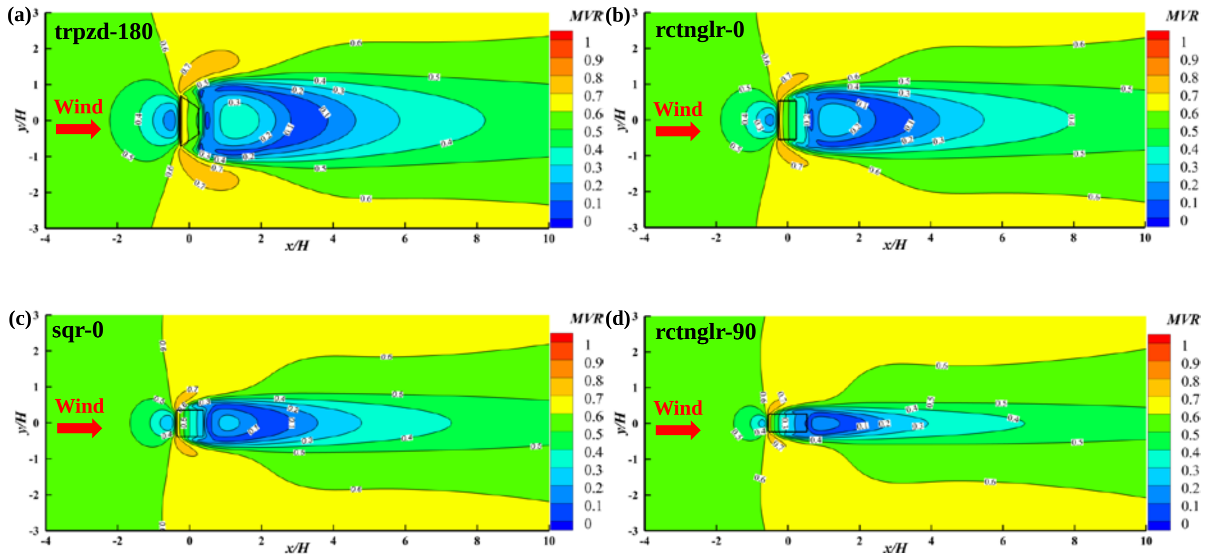

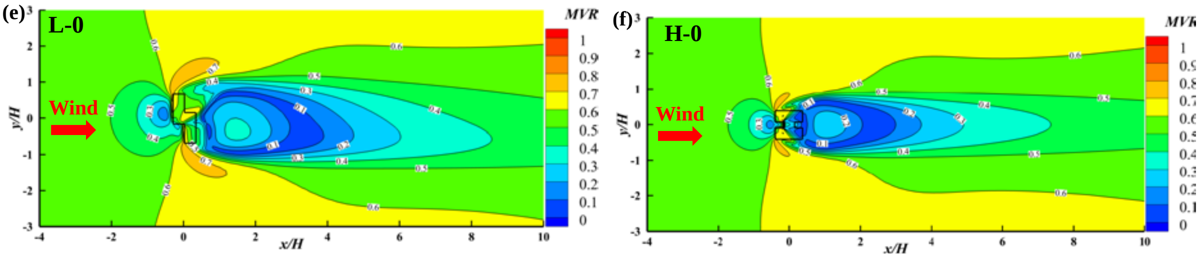

Fig. 9. Pedestrian-level *MVR* distributions around (a) trpzd-180 model, (b) rctnglr-0 model, (c) sqr-0 model, (d) rctnglr-90 model, (e) L-0 model, and (f) H-0 model.

4.4.3. Effects of building depth

The building depths (parallel to the incident wind) of the L-0, trpzd-180, rctnglr-0, sqr-0, H-0, and rctnglr-90 models are 16 m, 25 m, 25 m, 37 m, 38m, and 54 m, respectively. As shown in Fig. 9(a, b, e), the high wind velocity zone can be observed behind the buildings, which results from the sufficiently strong throughflow. Note that the downstream near-field high wind velocity zone is distinguished from the high wind velocity in the wind criterion category, and is named in contrast to the leeward wake zone. Similar phenomenon is not observed in Fig. 9(c, d, f). Nevertheless, there are *MVR* contours below 0.3 in the lift-up areas of the sqr-0, rctnglr-90, and H-0 models (Fig. 9(c, d, f)). In other words, unfavorable wind comfort zones occur beneath these lift-up buildings. It can be concluded that building depth impacts the pedestrian-level wind comfort in the lift-up area, and unfavorable wind comfort zone may occur underneath the lift-up buildings with deep building depth.

4.5. PLW comfort around slab-like models **(**AR_{UFWC} and AR_{HWV}**)**

4.5.1. Effects of converging flow and diverging flow

Slab-like models comprise two nonparallel identical slabs, which form a semi-open zone. This zone causes unique flow features around slab-like buildings. The contours of pedestrian-level *MVR* values around all slab-90 models at $\theta = 0°$, 90°, and 180° are given in Fig. 10. At $\theta = 0°$ (Fig. 10(a)), the semi-open zone is windward, converging and catching the wind flow, and the building functions as a wind shelter. Thus, a large unfavorable wind comfort zone is generated in the upstream near-field region by the strong wind-blocking effect, which is also pronounced around the corresponding lift-up building (Fig. 10(d)). At $\theta = 180°$ (Fig. 10(c)), the wind flow diverges along the two windward surfaces, and thus, the wind-blocking effect is less prominent and the upstream unfavorable wind comfort zone is small. However, because the semi-open zone is leeward, weak or calm wind is formed. As shown in Fig. 10(f), lift-up design substantially improves the wind comfort in the upstream and semi-open zones. The throughflow is sufficiently strong, thereby making the wind comfort in the entire semi-open zone acceptable. The building also exhibits less wind-blocking effects at $\theta = 90°$ (Fig. 10(b, e)), and thus, the upstream unfavorable wind comfort zone is smaller than that at $\theta = 0°$. Although the semi-open zone is leeward, its wind comfort is not as unfavorable as that at $\theta = 180°$.

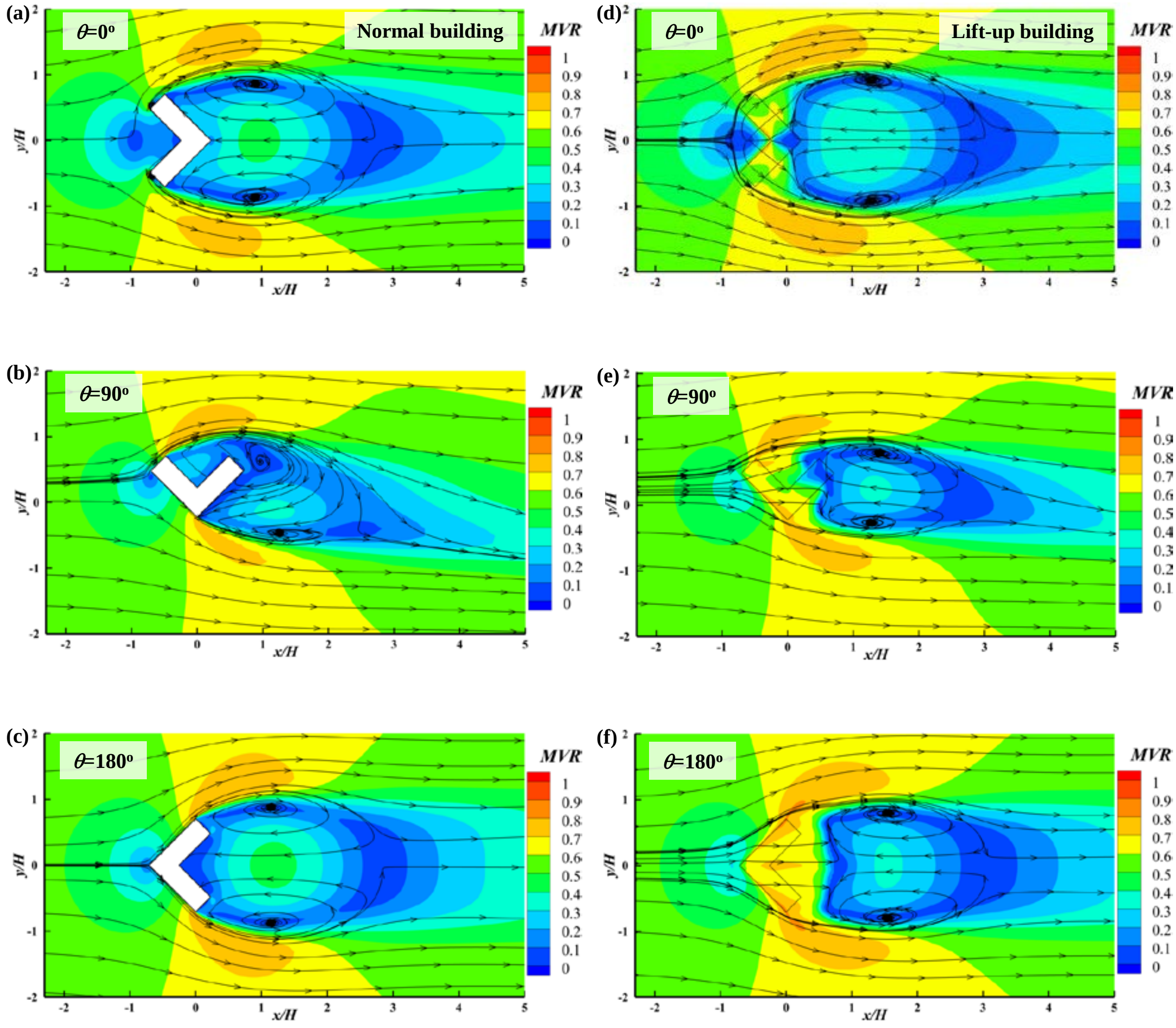

Fig. 10. Pedestrian-level *MVR* distributions around all slab-90 models: (a–c) normal buildings, (d–f) lift-up buildings under three wind directions.

Fig. 11 presents the AR_{UFWC} values in Regions XS and L for all slab-like models. For both normal and lift-up buildings, the near- and full-field AR_{UFWC} values at $\theta = 90°$ are the least among the three wind directions, indicating that this wind direction is most favorable for slab-like models. In the near field (Fig. 11(a–c)), the converging flow leads to ~41%–126% larger AR_{UFWC} values than the diverging flow in the lift-up buildings. The increments (~12%–35%) are less pronounced in the normal buildings. The findings suggest that the building has a better near-field PLW environment under diverging flow than under converging flow. Nevertheless, it is totally different in the full field (Fig. 11(d–f)), where the diverging flow results in greater AR_{UFWC} values than the converging flow, except for the slab-90 model. The differences are not as prominent as those in the near field, which are within 20%. The above results indicate that the diverging flow causes a larger area of unfavorable wind comfort in the downstream far-field zone than the converging flow.

The values of AR_{HWV} in Region L for all slab-like models are compared in Fig. 12. A lift-up building generally has higher AR_{HWV} values than the corresponding normal building. Besides, two mutual facts are observed for both normal and lift-up buildings. First, the AR_{HWV} value at $\theta = 90°$ is the smallest among those obtained in the three wind directions. This may be because the projected building width at $\theta = 90°$ is the smallest. Second, although the projected building widths at $\theta = 0°$ and 180° are equivalent, the AR_{HWV} value at $\theta = 180°$ is explicitly greater than that at $\theta = 0°$. The change percentages are ~31%–86% in normal buildings and ~9%–70% in lift-up buildings.

4.5.2. Effects of included angle

As shown in Fig. 11(d, f), the full-field AR_{UFWC} values show an ascent tendency with the increased included angle at $\theta = 0°$ and 180°. The normal (lift-up) slab-150 model has ~39% (~30%) greater area of unfavorable wind comfort zone AR_{UFWC} compared with the normal (lift-up) slab-90 model at $\theta = 0°$. The normal (lift-up) slab-150 model has ~70% (~63%) greater AR_{UFWC} value compared with the normal (lift-up) slab-90 model at $\theta = 180°$. On the contrary, there is a descend tendency at $\theta =$ 90° (Fig. 11(e)). The value of AR_{UFWC} for normal (lift-up) slab-90 model is over twofold (threefold) than that for normal (lift-up) slab-150 model. These can be explained by the fact that with the enlargement of the included angle, the projected width increases at $\theta = 0°$ and 180°, but decreases at $\theta = 90°$. Similar phenomenon can be observed from near-field AR_{UFWC} values (Fig. 11(a–c)). However, the variation in

AR_{UFWC} values among the lift-up slab-120, slab-135, and slab-150 models is very small; the change percentage is below 2% at $\theta = 0°$. Overall, at $\theta = 0°$ and 180°, the slab-like model with a smaller included angle exhibits smaller unfavorable wind comfort zone, while it is totally the opposite at $\theta = 90°$.

4.5.3. Effects of surface curvature

Unlike the slab-150 model, the two wide surfaces of the arc-150 model are curved. As shown in Figs. 11 and 12, the arc-150 model generally has lower AR_{UFWC} values but higher AR_{HWV} values as compared to the slab-150 model. The exception is that the near-field AR_{UFWC} value of the lift-up arc-150 model is 4.4% larger than that of the lift-up slab-150 model at $\theta = 0°$. Specifically, the differences in AR_{UFWC} values between the slab-150 and arc-150 models are remarkably lesser at $\theta = 0°$ and 180°. The variation percentage ranges from −4.4% to 6.4%. In contrast, the difference is more pronounced at $\theta = 90°$, which can reach a value of 14.7%. The results indicate that although the arc-150 model has a slightly smaller unfavorable wind comfort zone and a slightly larger high wind velocity zone than the slab-150 model, the difference in the PLW comfort caused by the surface curvature is not significant.

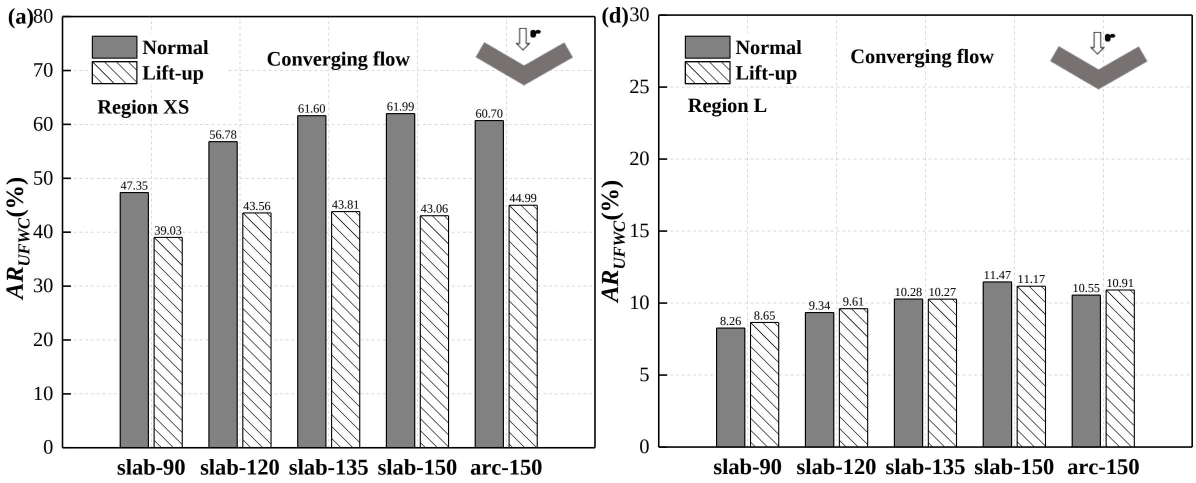

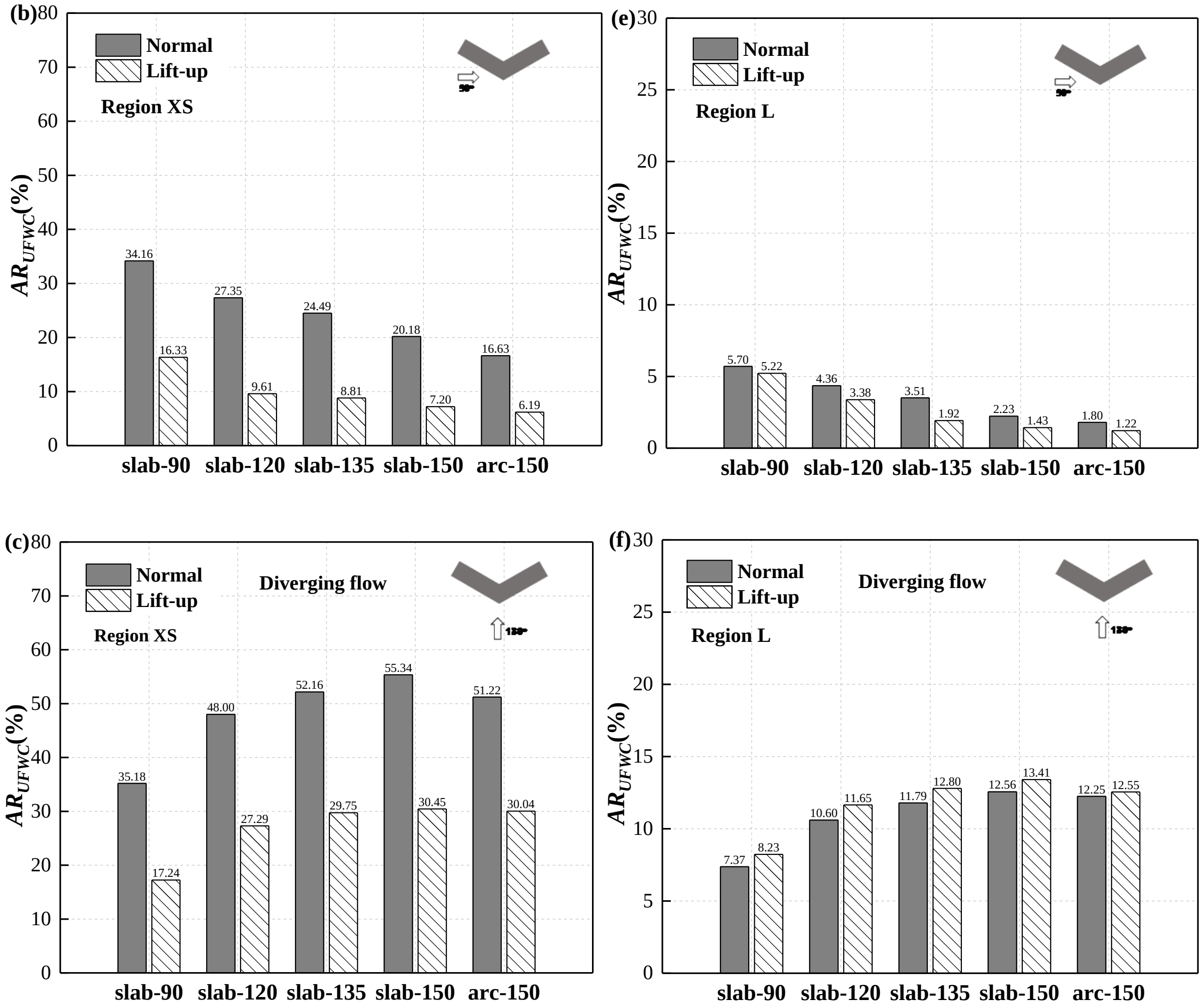

Fig. 11. AR_{UFWC} values in (a–c) Region XS and (d–f) Region L for all slab-like models at 0°, 90°, and 180°.

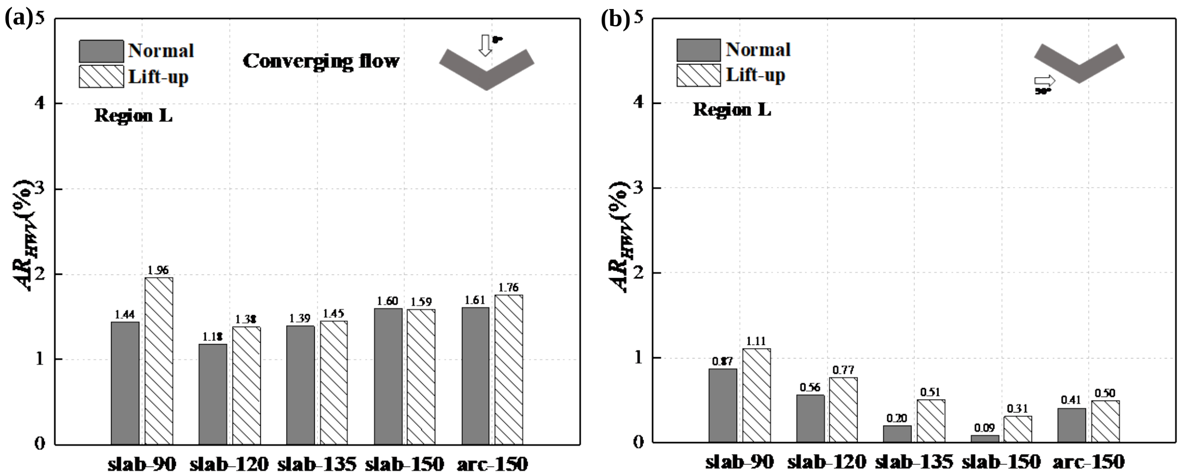

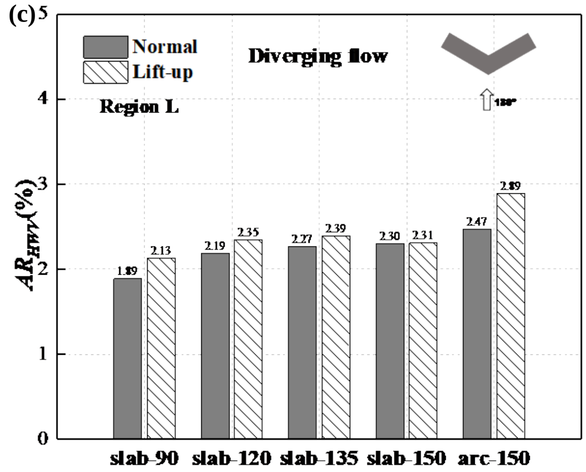

Fig. 12. AR_{HWV} values in Region L for all slab-like models under three wind directions: (a) $\theta = 0°$, (b) $\theta = 90°$, and (c) $\theta = 180°$.

4.6. PLW comfort around cruciform models (AR_{UFWC} and AR_{HWV})

Fig. 13 shows the values of AR_{UFWC} in Regions XS and L for all cruciform models at $\theta = 0°$, 22.5°, and 45°. For normal buildings, $\theta = 45°$ is the most favorable wind direction with the smallest AR_{UFWC} values and $\theta = 0°$ is the worst wind direction with the largest AR_{UFWC} values. Conversely, for lift-up buildings, the most favorable wind direction is $\theta = 0°$ and the least favorable is $\theta = 45°$. For both normal and lift-up buildings, the minimum full-field AR_{UFWC} values are found at $\theta = 45°$, while the maximum values are observed at $\theta = 0°$.

4.6.1. Effects of surface discontinuity

The crcfm-A, crcfm-B, and crcfm-C models are three variants of the basic cruciform building: crcfm model. Compared to the crcfm model, the crcfm-A model has slightly greater AR_{UFWC} values in most cases. However, the differences are insignificant, which are below 8%. The crcfm-B model has ~10%–26% smaller AR_{UFWC} values than the crcfm model at $\theta = 0°$. The lift-up design strengthens the differences. At $\theta = 22.5°$ and 45°, the differences of AR_{UFWC} values between the crcfm-B and crcfm models are not significant, which are below 5%. The crcfm-C model has smaller AR_{UFWC} values than the crcfm model in most cases, which are more pronounced at $\theta = 0°$ and 22.5°, especially for near-field AR_{UFWC} values. The decrements in near-field AR_{UFWC} values for lift-up buildings are up to ~73%

and 28% at $\theta = 0°$ and 22.5°, respectively. These results suggest that the crcfm-A model has a slightly larger unfavorable wind comfort zone than the crcfm model, while the crcfm-B and crcfm-C models have a smaller unfavorable wind comfort zone than the crcfm model. The lift-up design strengthens the benefits of crcm-B and crcm-C model in shrinking the unfavorable wind comfort zone. To some extent, the recessed corner modification of crcfm-B is beneficial for the PLW comfort around the building, despite the improvement is insignificant. Small cavities in the extended parts of the crcfm-A model aggrandize the discontinuity of the surface, thus adversely affecting the area of unfavorable wind comfort zone. The notches padding modification of the crcfm-C model moderates the surface discontinuity, thereby benefitting the PLW comfort.

To compare the comprehensive performances of four cruciform models under the various wind directions, the mean AR_{UFWC} values are calculated. The mean near-field AR_{UFWC} values are ~31.6%–35.5% for normal cruciform models and ~17.9%–24.4% for lift-up cruciform models. The mean full-field AR_{UFWC} values are ~6.1%–6.6% for normal cruciform models and ~6.2%–6.9% for lift-up cruciform models. The cruciform models can be referred as variants of the square model. As shown in Figs. 6(b) and 7(a), the near-field mean AR_{UFWC} values for normal and lift-up square models are ~28.5% and 19.1%, respectively; the full-field mean AR_{UFWC} values for normal and lift-up square models are 5.6% and 5.4%. By comparison, cruciform models have greater mean AR_{UFWC} values than the square model in most cases. This finding reveals that the cruciform models with uneven or discontinuous surfaces generally have a ~8% –28% larger unfavorable wind comfort zone than the square models with flat surfaces.

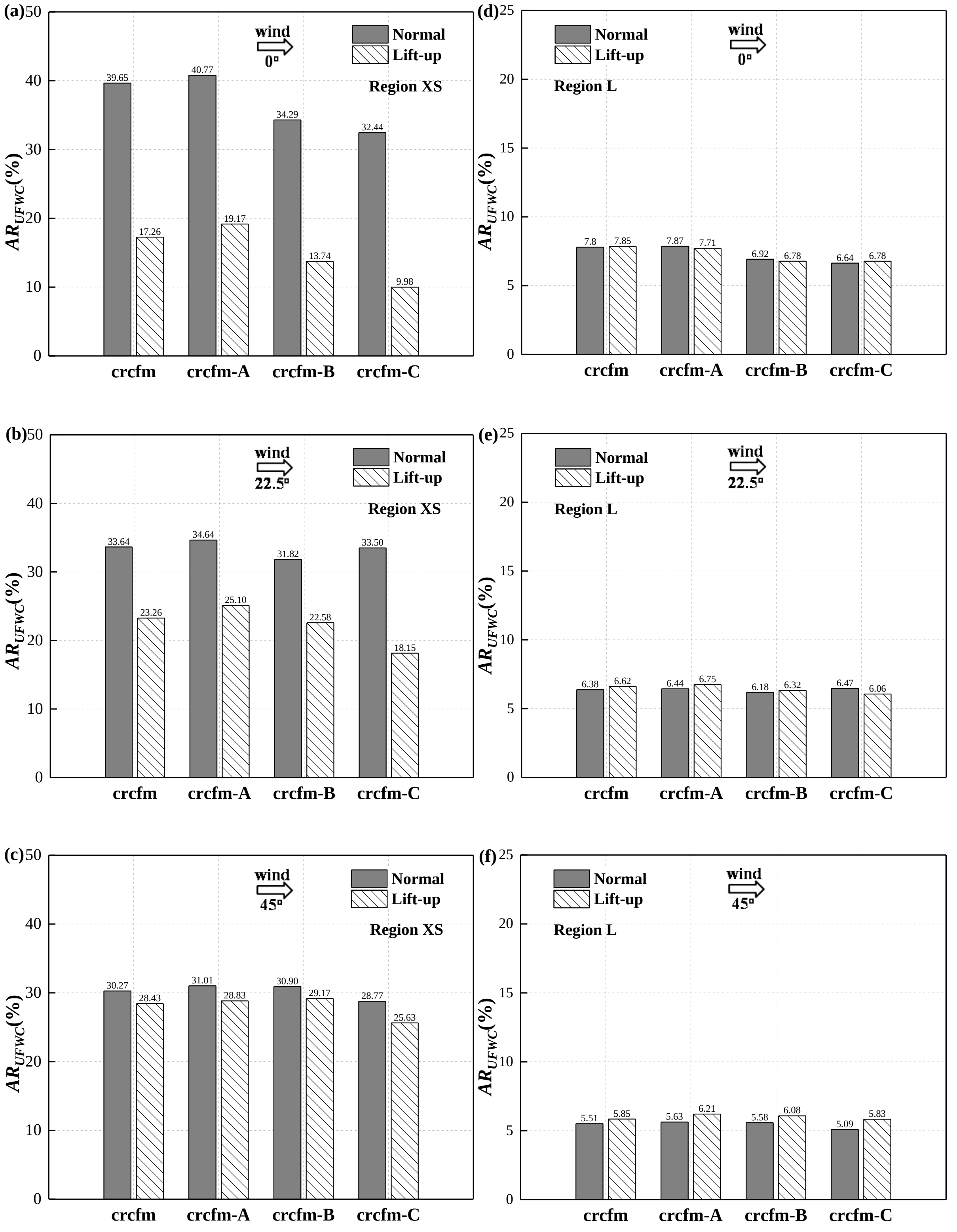

Fig. 13. AR_{UFWC} values in (a–c) Region XS and (d–f) Region L for all cruciform models at $\theta = 0°, 22.5°$, and 45°.

4.7. PLW comfort around trident models **(**AR_{UFWC} and AR_{HWV}**)**

4.7.1. Y model vs. T model

Fig. 14(a-b) shows the AR_{UFWC} values in Region XS and L for all trident models. "T-0" indicates the cases of the T model at $\theta = 0°$, while "Y-0" indicates those of the Y model at $\theta = 0°$. For normal buildings, the T model has greater near- and full-field AR_{UFWC} values than the Y model at $\theta = 0°$ and 180°; however, it is totally different at $\theta = 90°$, where the T model has smaller AR_{UFWC} values than the Y model. Compared to normal buildings, the difference of AR_{UFWC} values between lift-up T and Y models is less pronounced. To sum up, the Y model generally has a smaller unfavorable wind comfort zone than the T model under the parallel incident wind ($\theta = 0°$ and 180°), while the relationship is opposite under the perpendicular incident wind ($\theta = 90°$).

The values of AR_{HWV} for all trident models are shown in Fig. 14(c). For the Y model, the lift-up design improves AR_{HWV} values under three wind directions. For the T model, the impact of lift-up design on AR_{HWV} values is insignificant at $\theta = 0°$ and 90°. By comparison, the Y model has a greater area of high wind velocity zone than the T model at $\theta = 0°$ and 180° but a smaller area of high wind velocity zone than the T model at $\theta = 0°$.

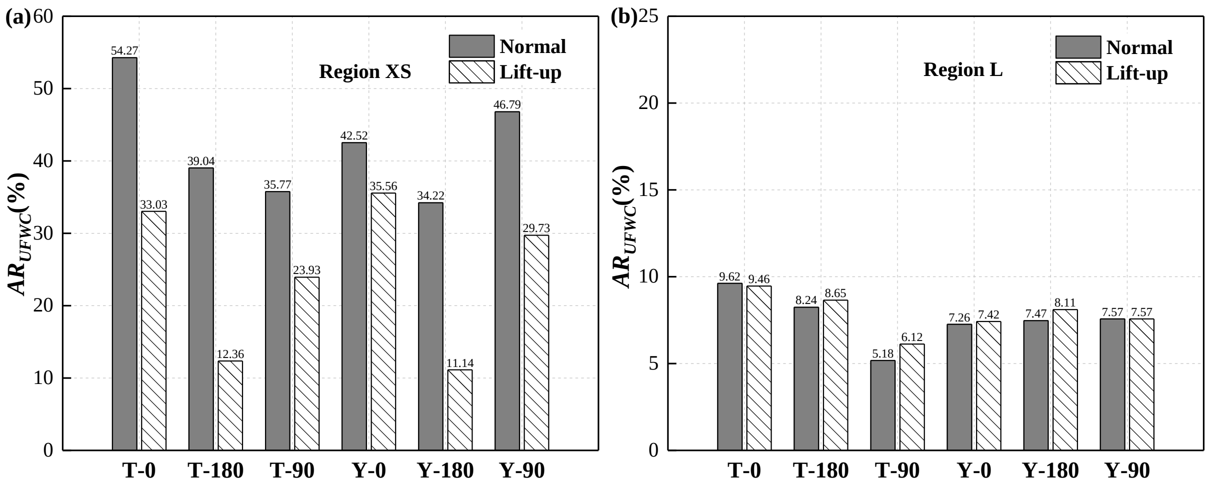

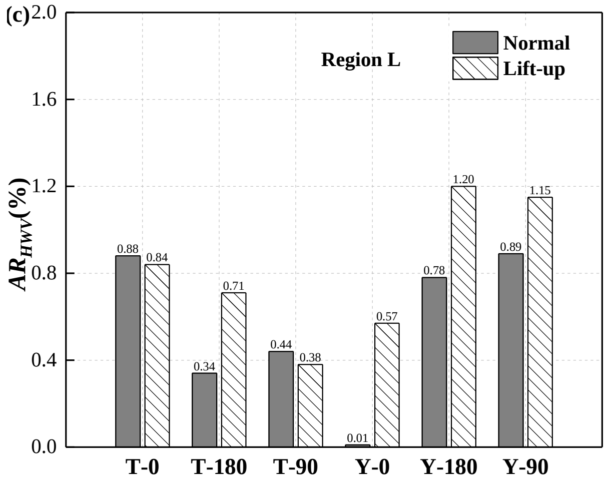

Fig. 14. AR_{UFWC} values in (a) Region XS and (b) Region L, (c) AR_{HWV} values in Region L for trident models.

5. Discussion

Lift-up design has proved improving the PLW comfort under weak wind condition by previous research, which was mainly based on the generically rectangular- or square-plan building models. This study focused on evaluating the PLW comfort around lift-up buildings with various unconventional configurations under weak wind conditions. The impacts of configuration parameters on the area of unfavorable wind comfort zone and lateral high wind velocity zone were quantitatively and systematically analyzed. We hoped to deliver a comprehensive evaluation method for PLW comfort around a specific shaped building. The area of unfavorable/acceptable wind comfort zone and the research region were thereby emphasized when analyzing the results. The size of the research region played an important role in assessing the impacts of lift-up design and building configuration. For example, from the view of full-field wind comfort, rounded configuration has the greatest acceptable wind comfort zone among polygonal buildings; however, from the view of near-field wind comfort, triangular or pentagonal configuration are more likely to provide a larger acceptable wind comfort zone. Therefore, whether the actual effects of a configuration are positive or negative sometimes depends on the interest precinct.

This study assumed the isolated building model and simplified lift-up building model without supporting structures in the lift-up areas. The objective was to eliminate other unexpected impacts on PLW comfort unrelated to the building configuration as much as possible, highlighting the effects of building configuration. Based on this assumption, our findings can be more representative of depicting the generic effects of building configuration on the PLW comfort around the lift-up building. In reality, the greening plants, recreation facilities, and pedestrians in the lift-up area, the surrounding buildings, and meteorological conditions can considerably influence the flow field around a lift-up building. The performances of the lift-up design and building configuration may be affected. All these factors should be considered in practical applications.

The mean wind velocity ratio was used as the wind comfort indicator because it was more representative for describing the actual wind environment than the gust wind velocity. Therefore, the SRANS approach was employed to predict the mean flow field. The validation test against wind tunnel data justified the satisfactory prediction accuracy of SRANS approach. However, SRANS approach could not provide instantaneous turbulent fluctuations, which might affect the PLW comfort. Future work will consider using the large eddy simulation (LES) model to study the turbulent fluctuation features around the lift-up building with various configurations.

6. Conclusions

A series of CFD simulations were conducted to investigate the PLW comfort around lift-up buildings with 22 unconventional configurations, derived from existing buildings in Hong Kong. The PLW comfort was categorized into unfavorable wind comfort, acceptable wind comfort, and unacceptable wind comfort according to *MVR* and wind comfort criterion. The area ratios of different wind comfort zones were calculated to quantify the wind comfort performance of a configuration. The tested configurations were classified into five groups: “polygonal,” “slab-like,” “cruciform,” “trident,” and “assembled.” Each category had unique aerodynamic features, and their relations with the PLW comfort and lift-up design’s performance were identified. The key findings of this study are summarized as follows:

(1). Lift-up design can considerably improve PLW comfort near buildings. However, the improvement efficiency is sensitive to the incident wind direction for most configurations and weakens with the size of the research region. Furthermore, the building configuration affects the performance of lift-up design to some extent.

(2). A positive correlation of the projected width with the sizes of unfavorable wind comfort and high wind velocity is identified. Moreover, the building depth proves to influence the PLW comfort in the lift-up area, leading to an unfavorable wind comfort zone. The throughflow weakens with the building depth.

(3). From the aspect of near-field wind comfort, the diverging flow is more beneficial than the converging flow because it leads to a larger acceptable wind comfort zone around the slab-like building.

(4). The included angle affects the PLW comfort and effectiveness of the lift-up design for the near-field wind comfort. With an increase in the included angle, the full-field acceptable wind comfort zone shrinks at $\theta = 0°$ and 180° but expands at $\theta = 90°$. The lift-up design has more efficient performance for improving the PLW comfort for slab-like building with a larger included angle.

(5). Although the arc-150 model with curved surfaces has a larger acceptable wind comfort zone than the slab-150 model with flat surfaces, the difference in the PLW comfort caused by the surface curvature is insignificant.

(6). The surface discontinuity has adverse effects on mean wind velocity. In most cases, cruciform models have a smaller acceptable wind comfort zone than square models. The crcfm model has a slightly greater acceptable wind comfort zone than the crcfm-A model but a smaller acceptable wind comfort zone than the crcfm-B and crcfm-C models.

This study provides an insight into the impacts of building configuration, incident wind direction, and precinct size on the effectiveness of the lift-up design. The findings can help architects and city planners determine an appropriate building configuration and orientation. Moreover, the evaluation method can be applied to other wind-related issues.

Acknowledgments

This work was supported by a PhD studentship funded by The Hong Kong Polytechnic University.

References

[1] Y. Du, C.M. Mak, K. Kwok, K.T. Tse, T.C. Lee, Z. Ai, J. Liu, J. Niu, New criteria for assessing low wind environment at pedestrian level in Hong Kong, Build. Environ. 123 (2017) 23-36, https://doi.org/10.1016/j.buildenv.2017.06.036.

[2] HKO (Hong Kong Observatory), Annual average of 12-hourly 10-minute mean wind speed of King's Park and Waglan Island (1968-2015). https://www.hko.gov.hk/en/climate_change/obs_hk_wind.htm.

[3] J. Hang, Y. Li, M. Sandberg, R. Buccolieri, S. Di Sabatino, The influence of building height variability on pollutant dispersion and pedestrian ventilation in idealized high-rise urban areas, Build. Environ. 56 (2012) 346-360, https://doi.org/10.1016/j.buildenv.2012.03.023.

[4] Z.T. Ai, C.M. Mak, Large eddy simulation of wind-induced interunit dispersion around multistory buildings, Indoor Air 26(2) (2016) 259-73, https://doi.org/10.1111/ina.12200.

[5] C. Sha, X. Wang, Y. Lin, Y. Fan, X. Chen, J. Hang, The impact of urban open space and 'lift-up' building design on building intake fraction and daily pollutant exposure in idealized urban models, Sci. Total Environ. 633 (2018) 1314-1328, https://doi.org/10.1016/j.scitotenv.2018.03.194.

[6] R. Buccolieri, M. Sandberg, S. Di Sabatino, City breathability and its link to pollutant concentration distribution within urban-like geometries, Atmos. Environ. 44(15) (2010) 1894-1903, https://doi.org/10.1016/j.atmosenv.2010.02.022.

[7] I. Panagiotou, M.K. Neophytou, D. Hamlyn, R.E. Britter, City breathability as quantified by the exchange velocity and its spatial variation in real inhomogeneous urban geometries: an example from central London urban area, Sci. Total Environ. 442 (2013) 466-77, https://doi.org/10.1016/j.scitotenv.2012.09.001.

[8] V. Cheng, E. Ng, C. Chan, B. Givoni, Outdoor thermal comfort study in a sub-tropical climate: a longitudinal study based in Hong Kong, Int. J. Biometeorol. 56(1) (2012) 43-56, https://doi.org/10.1007/s00484-010-0396-z.

[9] J. Liu, J. Niu, Q. Xia, Combining measured thermal parameters and simulated wind velocity to predict outdoor thermal comfort, Build. Environ. 105 (2016) 185-197, https://doi.org/10.1016/j.buildenv.2016.05.038.

[10] M. Lin, J. Hang, Y. Li, Z. Luo, M. Sandberg, Quantitative ventilation assessments of idealized urban canopy layers with various urban layouts and the same building packing density, Build. Environ. 79 (2014) 152-167, https://doi.org/10.1016/j.buildenv.2014.05.008.

[11] A.J. Arnfield, Two decades of urban climate research: a review of turbulence, exchanges of energy and water, and the urban heat island, Int J Climatol 23(1) (2003) 1-26, https://doi.org/10.1002/joc.859.

[12] R. Giridharan, S. Ganesan, S.S.Y. Lau, Daytime urban heat island effect in high-rise and high-density residential developments in Hong Kong, Energy Build. 36(6) (2004) 525-534, https://doi.org/10.1016/j.enbuild.2003.12.016.

[13] D. Lai, W. Liu, T. Gan, K. Liu, Q. Chen, A review of mitigating strategies to improve the thermal environment and thermal comfort in urban outdoor spaces, Sci. Total Environ. 661 (2019) 337-353, https://doi.org/10.1016/j.scitotenv.2019.01.062.

[14] Z. Zhang, T. Xue, X. Jin, Effects of meteorological conditions and air pollution on COVID-19 transmission: Evidence from 219 Chinese cities, Sci. Total Environ. 741 (2020) 140244, https://doi.org/10.1016/j.scitotenv.2020.140244.

[15] S.K. Pani, N.H. Lin, S. RavindraBabu, Association of COVID-19 pandemic with meteorological parameters over Singapore, Sci. Total Environ. 740 (2020) 140112, https://doi.org/10.1016/j.scitotenv.2020.140112.

[16] H. Xu, C. Yan, Q. Fu, K. Xiao, Y. Yu, D. Han, W. Wang, J. Cheng, Possible environmental effects on the spread of COVID-19 in China, Sci. Total Environ. 731 (2020) 139211, https://doi.org/10.1016/j.scitotenv.2020.139211.

[17] C. Lin, A.K.H. Lau, J.C.H. Fung, C. Guo, J.W.M. Chan, D.W. Yeung, Y. Zhang, Y. Bo, M.S. Hossain, Y. Zeng, X.Q. Lao, A mechanism-based parameterisation scheme to investigate the association between transmission rate of COVID-19 and meteorological factors on plains in China, Sci. Total Environ. 737 (2020) 140348, https://doi.org/10.1016/j.scitotenv.2020.140348.

[18] M. Ahmadi, A. Sharifi, S. Dorosti, S. Jafarzadeh Ghoushchi, N. Ghanbari, Investigation of effective climatology parameters on COVID-19 outbreak in Iran, Sci. Total Environ. 729 (2020) 138705, https://doi.org/10.1016/j.scitotenv.2020.138705.

[19] E.G. Gardner, D. Kelton, Z. Poljak, M. Van Kerkhove, S. von Dobschuetz, A.L. Greer, A case-crossover analysis of the impact of weather on primary cases of Middle East respiratory syndrome, BMC Infect. Dis. 19(1) (2019) 113, https://doi.org/10.1186/s12879-019-3729-5.

[20] Y. Cui, Z.F. Zhang, J. Froines, J. Zhao, H. Wang, S.Z. Yu, R. Detels, Air pollution and case fatality of SARS in the People's Republic of China: an ecologic study, Environ. Health 2(1) (2003) 15, https://doi.org/10.1186/1476-069X-2-15.

[21] J.L. Schulman, E.D. Kilbourne, Airborne transmission of influenza virus infection in mice, Nature 195 (1962) 1129-30, https://doi.org/10.1038/1951129a0.

[22] HKO (Hong Kong Observatory), Annual mean temperature recorded at the Hong Kong Observatory Headquarters (1885-2019). https://www.hko.gov.hk/en/climate_change/obs_hk_temp.htm.

[23] E. Ng, Policies and technical guidelines for urban planning of high-density cities - air ventilation assessment (AVA) of Hong Kong, Build. Environ. 44(7) (2009) 1478-1488, https://doi.org/10.1016/j.buildenv.2008.06.013.

[24] T. van Druenen, T. van Hooff, H. Montazeri, B. Blocken, CFD evaluation of building geometry modifications to reduce pedestrian-level wind speed, Build. Environ. 163 (2019), https://doi.org/10.1016/j.buildenv.2019.106293.

[25] L. Chen, J. Hang, M. Sandberg, L. Claesson, S. Di Sabatino, H. Wigo, The impacts of building height variations and building packing densities on flow adjustment and city breathability in idealized urban models, Build. Environ. 118 (2017) 344-361, https://doi.org/10.1016/j.buildenv.2017.03.042.

[26] R. Ramponi, B. Blocken, L.B. de Coo, W.D. Janssen, CFD simulation of outdoor ventilation of generic urban configurations with different urban densities and equal and unequal street widths, Build. Environ. 92 (2015) 152-166, https://doi.org/10.1016/j.buildenv.2015.04.018.

[27] F. Yang, Y. Gao, K. Zhong, Y. Kang, Impacts of cross-ventilation on the air quality in street canyons with different building arrangements, Build. Environ. 104 (2016) 1-12, https://doi.org/10.1016/j.buildenv.2016.04.013.

[28] Y.M. Su, H.T. Chang, Influence of Summer Outdoor Pedestrian Wind Environment Comfort with Height-to-Width Ratios of Arcade in Taiwan, Applied Mechanics and Materials 851 (2016) 633-638, https://doi.org/10.4028/www.scientific.net/AMM.851.633.

[29] Y.-H. Juan, A.-S. Yang, C.-Y. Wen, Y.-T. Lee, P.-C. Wang, Optimization procedures for enhancement of city breathability using arcade design in a realistic high-rise urban area, Build. Environ. 121 (2017) 247-261, https://doi.org/10.1016/j.buildenv.2017.05.035.

[30] C.-Y. Wen, Y.-H. Juan, A.-S. Yang, Enhancement of city breathability with half open spaces in ideal urban street canyons, Build. Environ. 112 (2017) 322-336, https://doi.org/10.1016/j.buildenv.2016.11.048.

[31] K.T. Tse, X. Zhang, A.U. Weerasuriya, S.W. Li, K.C.S. Kwok, C.M. Mak, J. Niu, Adopting 'lift-up' building design to improve the surrounding pedestrian-level wind environment, Build. Environ. 117 (2017) 154-165, https://doi.org/10.1016/j.buildenv.2017.03.011.

[32] Q. Xia, X. Liu, J. Niu, K.C.S. Kwok, Effects of building lift-up design on the wind environment for pedestrians, Indoor Built Environ 26(9) (2015) 1214-1231, https://doi.org/10.1177/1420326x15609967.

[33] Y. Du, C.M. Mak, J. Liu, Q. Xia, J. Niu, K.C.S. Kwok, Effects of lift-up design on pedestrian level wind comfort in different building configurations under three wind directions, Build. Environ. 117 (2017) 84-99, https://doi.org/10.1016/j.buildenv.2017.03.001.

[34] X. Zhang, K.T. Tse, A.U. Weerasuriya, S.W. Li, K.C.S. Kwok, C.M. Mak, J. Niu, Z. Lin, Evaluation of pedestrian wind comfort near 'lift-up' buildings with different aspect ratios and central core modifications, Build. Environ. 124 (2017) 245-257, https://doi.org/10.1016/j.buildenv.2017.08.012.

[35] J. Liu, X. Zhang, J. Niu, K.T. Tse, Pedestrian-level wind and gust around buildings with a 'lift-up' design: Assessment of influence from surrounding buildings by adopting LES, Build Simul 12(6) (2019) 1107-1118, https://doi.org/10.1007/s12273-019-0541-5.

[36] L.W. Chew, L.K. Norford, Pedestrian-level wind speed enhancement in urban street canyons with void decks, Build. Environ. 146 (2018) 64-76, https://doi.org/10.1016/j.buildenv.2018.09.039.

[37] L.W. Chew, L.K. Norford, Pedestrian-level wind speed enhancement with void decks in three-dimensional urban street canyons, Build. Environ. 155 (2019) 399-407, https://doi.org/10.1016/j.buildenv.2019.03.058.

[38] K. Zhang, G. Chen, X. Wang, S. Liu, C.M. Mak, Y. Fan, J. Hang, Numerical evaluations of urban design technique to reduce vehicular personal intake fraction in deep street canyons, Sci. Total Environ. 653 (2019) 968-994, https://doi.org/10.1016/j.scitotenv.2018.10.333.

[39] K. Zhang, G. Chen, Y. Zhang, S. Liu, X. Wang, B. Wang, J. Hang, Integrated impacts of turbulent mixing and NOX-O3 photochemistry on reactive pollutant dispersion and intake fraction in shallow and deep street canyons, Sci. Total Environ. 712 (2020) 135553, https://doi.org/10.1016/j.scitotenv.2019.135553.

[40] M. Fan, C.K. Chau, E.H.W. Chan, J. Jia, A decision support tool for evaluating the air quality and wind comfort induced by different opening configurations for buildings in canyons, Sci. Total Environ. 574 (2017) 569-582, https://doi.org/10.1016/j.scitotenv.2016.09.083.

[41] ASHRAE, ASHRAE Standard 55: Thermal Environmental Conditions for Human Occupancy, ASHRAE, 2013, p. 54.

[42] J. Niu, J. Liu, T.-c. Lee, Z. Lin, C. Mak, K.-T. Tse, B.-s. Tang, K.C.S. Kwok, A new method to assess spatial variations of outdoor thermal comfort: Onsite monitoring results and implications for precinct planning, Build. Environ. 91 (2015) 263-270, https://doi.org/10.1016/j.buildenv.2015.02.017.

[43] Y. Du, C.M. Mak, T. Huang, J. Niu, Towards an integrated method to assess effects of lift-up design on outdoor thermal comfort in Hong Kong, Build. Environ. 125 (2017) 261-272, https://doi.org/10.1016/j.buildenv.2017.09.001.

[44] X. Zhang, K.T. Tse, A.U. Weerasuriya, K.C.S. Kwok, J. Niu, Z. Lin, C.M. Mak, Pedestrian-level wind conditions in the space underneath lift-up buildings, J. Wind. Eng. Ind. Aerodyn. 179 (2018) 58-69, https://doi.org/10.1016/j.jweia.2018.05.015.

[45] Y. Du, C.M. Mak, Y. Li, Application of a multi-variable optimization method to determine lift-up design for optimum wind comfort, Build. Environ. 131 (2018) 242-254, https://doi.org/10.1016/j.buildenv.2018.01.012.

[46] Y. Du, C.M. Mak, B.S. Tang, Effects of building height and porosity on pedestrian level wind comfort in a high-density urban built environment, Build Simul 11(6) (2018) 1215-1228, https://doi.org/10.1007/s12273-018-0451-y.

[47] Y. Du, C.M. Mak, Y. Li, A multi-stage optimization of pedestrian level wind environment and thermal comfort with lift-up design in ideal urban canyons, Sustain. Cities Soc. 46 (2019), https://doi.org/10.1016/j.scs.2019.101424.

[48] J. Liu, J. Niu, C.M. Mak, Q. Xia, Detached eddy simulation of pedestrian-level wind and gust around an elevated building, Build. Environ. 125 (2017) 168-179, https://doi.org/10.1016/j.buildenv.2017.08.031.

[49] T.R. Oke, Boundary layer climates, Routledge, 2002.

[50] X. Zhang, A.U. Weerasuriya, B. Lu, K.T. Tse, C.H. Liu, Y. Tamura, Pedestrian-level wind environment near a super-tall building with unconventional configurations in a regular urban area, Build Simul 13(2) (2019) 439-456, https://doi.org/10.1007/s12273-019-0588-3.

[51] X. Xu, Q. Yang, A. Yoshida, Y. Tamura, Characteristics of pedestrian-level wind around super-tall buildings with various configurations, J. Wind. Eng. Ind. Aerodyn. 166 (2017) 61-73, https://doi.org/10.1016/j.jweia.2017.03.013.

[52] H. Tanaka, Y. Tamura, K. Ohtake, M. Nakai, Y. Chul Kim, Experimental investigation of aerodynamic forces and wind pressures acting on tall buildings with various unconventional configurations, J. Wind. Eng. Ind. Aerodyn. 107-108 (2012) 179-191, https://doi.org/10.1016/j.jweia.2012.04.014.

[53] C.W. Tsang, K.C.S. Kwok, P.A. Hitchcock, Wind tunnel study of pedestrian level wind environment around tall buildings: Effects of building dimensions, separation and podium, Build. Environ. 49 (2012) 167-181, https://doi.org/10.1016/j.buildenv.2011.08.014.

[54] Y. Tominaga, A. Mochida, R. Yoshie, H. Kataoka, T. Nozu, M. Yoshikawa, T. Shirasawa, AIJ guidelines for practical applications of CFD to pedestrian wind environment around buildings, J. Wind. Eng. Ind. Aerodyn. 96(10-11) (2008) 1749-1761, https://doi.org/10.1016/j.jweia.2008.02.058.

[55] Z.T. Ai, C.M. Mak, Potential use of reduced-scale models in CFD simulations to save numerical resources: Theoretical analysis and case study of flow around an isolated building, J. Wind. Eng. Ind. Aerodyn. 134 (2014) 25-29, https://doi.org/10.1016/j.jweia.2014.08.009.

[56] R. Meroney, Wind tunnel and numerical simulation of pollution dispersion: a hybrid approach, Paper for Invited Lecture at the Croucher Advanced Study Institute, Hong Kong University of Science and Technology (2004) 6-10,

[57] J. Franke, A. Hellsten, H. Schlünzen, B. Carissimo, D. Grawe, I. Goricsán, Z.k. JbHour, A. Karppinen, Best practice guideline for the CFD simulation of flows in the urban environment, 2007.

[58] J. Franke, A. Hellsten, K.H. Schlunzen, B. Carissimo, The COST 732 Best Practice Guideline for CFD simulation of flows in the urban environment: a summary, Int J Environ Pollut 44(1/2/3/4) (2011), https://doi.org/10.1504/ijep.2011.038443.

[59] B. Blocken, T. Stathopoulos, J. Carmeliet, CFD simulation of the atmospheric boundary layer: wall function problems, Atmos. Environ. 41(2) (2007) 238-252, https://doi.org/10.1016/j.atmosenv.2006.08.019.

[60] Fluent, ANSYS FLUENT 13.0 Theory Guide, Turbulence, ANSYS Inc, Canonsburg, PA, 2010.

[61] B. Blocken, T. Stathopoulos, J.P.A.J. van Beeck, Pedestrian-level wind conditions around buildings: Review of wind-tunnel and CFD techniques and their accuracy for wind comfort assessment, Build. Environ. 100 (2016) 50-81, https://doi.org/10.1016/j.buildenv.2016.02.004.

[62] B. Blocken, 50 years of Computational Wind Engineering: Past, present and future, J. Wind. Eng. Ind. Aerodyn. 129 (2014) 69-102, https://doi.org/10.1016/j.jweia.2014.03.008.

[63] T.-H. Shih, W.W. Liou, A. Shabbir, Z. Yang, J. Zhu, A new k-ϵ eddy viscosity model for high reynolds number turbulent flows, Comput Fluids 24(3) (1995) 227-238, https://doi.org/10.1016/0045-7930(94)00032-t.

[64] X. Zheng, H. Montazeri, B. Blocken, CFD simulations of wind flow and mean surface pressure for buildings with balconies: Comparison of RANS and LES, Build. Environ. 173 (2020), https://doi.org/10.1016/j.buildenv.2020.106747.

[65] B. Blocken, J. Carmeliet, Pedestrian wind conditions at outdoor platforms in a high-rise apartment building: generic sub-configuration validation, wind comfort assessment and uncertainty issues, Wind. Struct. An Int. J. 11(1) (2008) 51-70, https://doi.org/10.12989/was.2008.11.1.051.

[66] B. Blocken, J. Persoon, Pedestrian wind comfort around a large football stadium in an urban environment: CFD simulation, validation and application of the new Dutch wind nuisance standard, J. Wind. Eng. Ind. Aerodyn. 97(5-6) (2009) 255-270, https://doi.org/10.1016/j.jweia.2009.06.007.

[67] A. Ricci, I. Kalkman, B. Blocken, M. Burlando, M.P. Repetto, Impact of turbulence models and roughness height in 3D steady RANS simulations of wind flow in an urban environment, Build. Environ. 171 (2020), https://doi.org/10.1016/j.buildenv.2019.106617.

[68] B. Blocken, P. Moonen, T. Stathopoulos, J. Carmeliet, Numerical Study on the Existence of the Venturi Effect in Passages between Perpendicular Buildings, J Eng Mech 134(12) (2008) 1021-1028, https://doi.org/10.1061/(Asce)0733-9399(2008)134:12(1021).

[69] H. Mittal, A. Sharma, A. Gairola, Numerical simulation of pedestrian level wind flow around buildings: Effect of corner modification and orientation, J. Build. Eng. 22 (2019) 314-326, https://doi.org/10.1016/j.jobe.2018.12.014.

[70] B. Blocken, W.D. Janssen, T. van Hooff, CFD simulation for pedestrian wind comfort and wind safety in urban areas: General decision framework and case study for the Eindhoven University campus, Environ Model Softw 30 (2012) 15-34, https://doi.org/10.1016/j.envsoft.2011.11.009.

[71] W.D. Janssen, B. Blocken, T. van Hooff, Pedestrian wind comfort around buildings: Comparison of wind comfort criteria based on whole-flow field data for a complex case study, Build. Environ. 59 (2013) 547-562, https://doi.org/10.1016/j.buildenv.2012.10.012.

[72] Y. Tominaga, A. Mochida, S. Murakami, S. Sawaki, Comparison of various revised k–ε models and LES applied to flow around a high-rise building model with 1:1:2 shape placed within the surface boundary layer, J. Wind. Eng. Ind. Aerodyn. 96(4) (2008) 389-411, https://doi.org/10.1016/j.jweia.2008.01.004.

[73] S.D. Sabatino, R. Buccolieri, H.R. Olesen, M. Ketzel, R. Berkowicz, J. Franke, M. Schatzmann, K.H. Schlunzen, B. Leitl, R. Britter, C. Borrego, A.M. Costa, S.T. Castelli, T.G. Reisin, A. Hellsten, J. Saloranta, N. Moussiopoulos, F. Barmpas, K. Brzozowski, I. Goricsan, M. Balczo, J.G. Bartzis, G. Efthimiou, J.L. Santiago, A. Martilli, M. Piringer, K.B. Stanzer, M. Hirtl, A.A. Baklanov, R.B. Nuterman, A.V. Starchenko, COST 732 in practice: the MUST model evaluation exercise, International Journal of Environment and Pollution 44(1/2/3/4) (2011), https://doi.org/10.1504/ijep.2011.038442.

[74] H.O. Michael Schatzmann, Jörg Franke, COST 732 Model Evaluation Case Studies: Approach and Results, COST Office, Brussels, Belgium, 2010.

[75] S.R. Hanna, O.R. Hansen, S. Dharmavaram, FLACS CFD air quality model performance evaluation with Kit Fox, MUST, Prairie Grass, and EMU observations, Atmospheric Environment 38(28) (2004) 4675-4687, https://doi.org/10.1016/j.atmosenv.2004.05.041.

[76] HKHA (Hong Kong Housing Authority), Standard Block Typical Floor Plans. https://www.housingauthority.gov.hk/en/global-elements/estate-locator/standard-block-typical-floor-plans/index.html.

[77] B. Blocken, J. Carmeliet, T. Stathopoulos, CFD evaluation of wind speed conditions in passages between parallel buildings—effect of wall-function roughness modifications for the atmospheric boundary layer flow, J. Wind. Eng. Ind. Aerodyn. 95(9-11) (2007) 941-962, https://doi.org/10.1016/j.jweia.2007.01.013.

[78] B. Blocken, T. Stathopoulos, J. Carmeliet, Wind environmental conditions in passages between two long narrow perpendicular buildings, J Aerosp Eng 21(4) (2008) 280-287, https://doi.org/10.1061/(Asce)0893-1321(2008)21:4(280).

[79] B. Li, Z. Luo, M. Sandberg, J. Liu, Revisiting the 'Venturi effect' in passage ventilation between two non-parallel buildings, Build. Environ. 94 (2015) 714-722, https://doi.org/10.1016/j.buildenv.2015.10.023.

[80] T.R. Oke, G. Mills, A. Christen, J.A. Voogt, Urban Climates, Cambridge: Cambridge University Press, 2017.

[81] N. Isyumov, A. Davenport, The ground level wind environment in built-up areas, Proceedings of the 4th International Conference on Wind Effects on Buildings and Structures,(Heathrow 1975), pp. 403-422.

[82] A.D. Penwarden, Acceptable wind speeds in towns, Building Science 8(3) (1973) 259-267, https://doi.org/10.1016/0007-3628(73)90008-x.